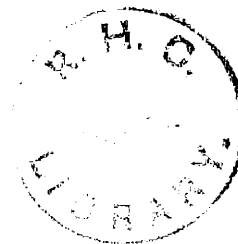OPTICAL STUDIES ON SMOOTH PLASTIC AND METAL SURFACES

SUBJECTED TO HIGH SPEED IMPACT

BY

THOMAS ROSSLYN BARNETT

THESIS
PRESENTED FOR THE DEGREE OF
DOCTOR OF PHILOSOPHY
IN THE UNIVERSITY OF LONDON

Royal Holloway College   June 1957.

ProQuest Number: 10096619

ProQuest 10096619

ABSTRACT

The deformation of plastics and metals is discussed
with reference to the effect of the rate of strain. A
review of the impact of solids is made, including elastic
and plastic wave propagation and the effect of the
reflection and superposition of the waves on the progress
of the impact. An account of the concepts underlying the
Hertz theory of impact is given, together with a
consideration of its applicability to the present work.
The various theories proposed for liquid-solid impact are
reviewed and discussed with reference to recent
experimental evidence.

An air gun and velocity measuring apparatus were
constructed for producing impacts and the theory and
practice of the optical techniques used for the examination
and measurement of the resultant surface distortions is
reviewed.

The damage sites produced by the impact of solid
spheres, deformable pellets and water drops on Perspex and
metals are studied, at striking velocities up to 1250 ft./sec.
(850 m.p.h.). This enables the complex process of the
impact of a deformable solid (or liquid) to be compared
with that of a hard solid. The main quantitative results
obtained for all the impact phenomena investigated relate
to the variation of the diameter and volume of the damaged
region with the velocity of impact.

In the case of steel ball impact on Perspex the diameter/velocity relation is similar to that calculated for elastic solid impact using Hertz's theory. For steel balls on Duralumin the volume of the indentation is proportional to the kinetic energy of the impactor.

The nature of the damage produced by polythene pellets and water drops is similar, but the rate of size increase with velocity is much greater than in solid-solid impact. This rapid variation is discussed in relation to the dynamic properties of the liquid and the solid.

A detailed examination of the surface damage is made including a measurement of the depths of the cracks in Perspex. Single and multiple drop impact are compared by studying a specimen subjected to artificial rain.

The changes in the type of depression observed when Perspex is impacted at different temperatures are analysed.

C O N T E N T S.

CHAPTER 1

INTRODUCTION

Interest in the phenomenon of liquid drop impact has increased in recent years because of the damage occurring to the leading edge of aircraft components when flying at a high speed through rain. Earlier workers in the field (mainly German and Swiss) were concerned with erosion in steam turbines due to the droplets present in wet steam. Now with the emphasis on the aircraft case and with less robust materials, higher velocities and larger drops, damage can occur in relatively short periods of time, indeed a single impact can cause appreciable damage.

The early work mentioned above was carried out using multiple impact techniques such as whirling the specimen on a wheel through a water jet, for periods varying from minutes to hours. The damage occurring was often due to a combination of mechanical and corrosive effects and considerations of fatigue strength were important, the materials being hard metals.

The present work is concerned with the measurement of the damage caused by the impact of a single drop, on the surfaces of plastics and softer metals, and with obtaining information about the impact phenomena as a whole. A single impact technique has been used, and precise measurements of the surface distortions which occur have been made using multiple beam interferometry.

Consider the impact of a liquid drop on a surface. As the impact velocity is increased, the drop will behave more like an elastic solid, although it retains its flow properties. Hence an elastic solid approach to high speed drop impact is considered to be a reasonable method of attack. Since, however, the phenomenon is a very complicated one, it was considered that studies of actual elastic solid impact in a similar velocity range would provide useful information, and possibly lead to a better understanding of the processes involved in liquid drop impact. The intermediate case of impact by a solid which is easily deformable is also studied.

The two methods of approach to the elastic impact of solids are considered. The first attempts were made by St. Venant (1867) and Boussinesq (1883). They discussed the longitudinal impact of two flat-ended bars, in terms of the elastic waves propogated through them. The other approach to the problem was the theory developed by Hertz (1881). He regarded the impact as a static effect and considered that the stresses and strains set up in the region of contact were the main factors determining the progress of the impact. Since both ideas are relevant to the impact of small particles in the velocity range considered here, they are discussed in detail.

The various theories developed for estimating the pressures involved in liquid drop impact are also discussed, though here the experimental data available are small.

As a result of these ideas and the experiments performed, the author feels that the wave motion in the drop must be considered in discussing the impact, but that the magnitude of the damage on the impacted surface can be described in terms of the Hertzian theory, since spherical waves are involved with a consequent falling off in amplitude, making the wave motion relatively unimportant. This would not apply if very large impact forces were considered. In any case, when discussing the mechanism of protection by very thin rubber coatings a consideration of the wave motion is essential.

The above assumption enables a quantitative estimate of the size of the damage site to be made, since the Hertz theory is the only approach developed for studying the non-uniaxial case.

One other factor which may be of importance, particularly at the higher velocities, is the rise time of the stress pulse initiated by the impact. This would affect the mechanism of response of plastic materials and possibly metals since a delay time for plastic flow occurs (Clark and Wood 1949).

There are other physical properties of the drop which may be relevant, such as viscosity and surface tension. An attempt to include some of these variables by treating the problem by means of dimensional analysis has been made by Engel (1955), but in order to get to an expression which

may be verified experimentally, many drastic assumptions have
to be made, and a very large amount of experimentá work will
be needed to test the equations.   The present work constitutes
an attempt to compare and contrast the impact of a liquid
drop and an elastic solid with the limited resources and time
available.

CHAPTER 2

DEFORMATION OF HIGH POLYMERS

2.1 STRESS STRAIN CURVE

Studies of stress strain curves of plastics have shown that the rate of strain has a marked effect on the curve. In general the yield stress and ultimate stress increase, and the ultimate elongation decreases with an increase in the testing speed.

This is shown in fig. 2.1. Up to the point A, the strain rate was low. Then the strain rate was increased fivefold which gave a sudden increase in the slope of the curve. Thus at the increased rate of straining a higher stress energy level must be applied to permit the bond mechanism of flow to relax. The temperature is also important, an increase in temperature acting like a decrease in the strain rate.

2.2 MECHANISM OF DEFORMATION

The mechanism of deformation of amorphous linear polymers (e.g. "Perspex) depends on the long chain structure of the molecule. Rotation about single valence bonds gives . flexibility to the molecule. Diffusion can occur as in liquids but only segments (i.e. 20-30 atoms) move. The resultant effect is that the polymer molecule as a whole wanders about (macro-Brownian movement) and the molecule changes its shape (micro-Brownian movement). On applying a shear stress the diffusion process is biased. The stress
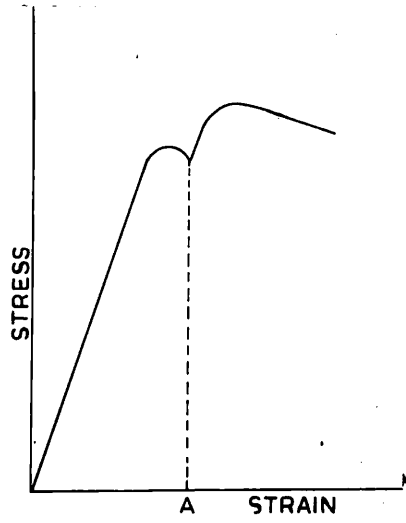
Fig. 2.1
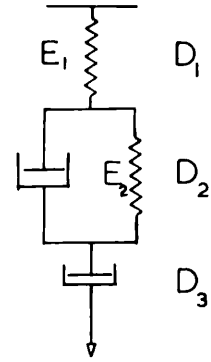
Fig. 2.2
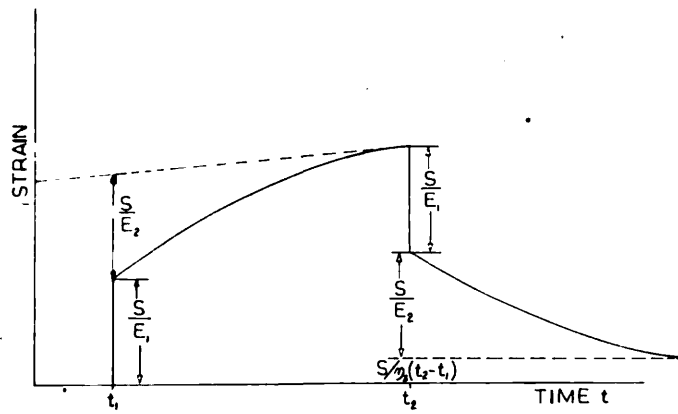
Fig. 2.3

biased macro-Brownian movement is a true flow, the biased

micro-Brownian movement is a retarded elasticity.   Thus the

total deformation mechanism can be summarised as

D(1)   The Instantaneous elastic deformation of Bond angles.

D(2)   The, Retarded elasticity due to change of shape.

D(3)   Flow.

D(1) is instantaneous and recoverable.

D(2) is time dependent and **depends** on the relaxation times

of the bonds involved.   These relaxation times are in turn,

temperature and stress energy dependent.   D(3) depends on

the relaxation of secondary bonds, but differs in that it is

not recoverable.

2.3 MECHANICAL MODELS.

The deformation mechanisms can be represented by a series

of mechanical elements fig.(2.2).   Alfrey (1948).

D_1 can be represented by a spring.

D_2 by a spring and dashpot in parallel.

D_3 by a dashpot.

D_1 is linear if Hookes law is obeyed and

$$\text{the Strain} = \frac{\text{Stress}}{E_1}$$

where E_1 = Modulus of Elasticity of the spring.

D_2 is known as a Voigt model, and its response to a stress

S is given by,

$$\epsilon = \frac{S}{E_2}\left(1-e^{-t/\lambda_2}\right)$$

where t = time of loading, E_2 = Modulus of spring, λ_2 = Relaxation time of the dashpot = η_1/E_2 where η_1 is the viscosity of the liquid in the dashpot, assumed Newtonian. E_2 will be considerably less than E_1.

Thus when t is small, $\epsilon \rightarrow 0$

when $t \rightarrow \infty$, $\epsilon \rightarrow S/E_2$.

D_3 is a dashpot containing a Newtonian liquid,

$$\text{Strain} = \frac{S.t}{\eta_2}$$

η_2 = Coefficient of Viscosity of Dashpot.

The elements D_1 and D_3 in series form a Maxwell model, which responds to a stress thus,

$$\frac{dS}{dt} = E_1\frac{d\epsilon}{dt} - \frac{S}{\lambda_3}$$

where λ_3 = Relaxation time of the dashpot.

Integrating at constant stress,

$$\epsilon = \frac{S}{E_1} + \frac{S}{E_1\lambda_3}.t$$

Hence the total deformation of the model is given by,

$$\epsilon = \frac{S}{E_1} + \frac{S}{E_2}\left(1 - e^{-t/\lambda_2}\right) + \frac{S}{E_1}.\frac{t}{\lambda_3}$$

It follows that the strain is dependent on the rate of loading and the two relaxation times λ_2 and λ_3. For most materials, λ_2 is much shorter than λ_3. The theoretical strain-time curve (under constant stress) is shown in fig. (2.3).

In addition, any of the elements may be non-linear, i.e. the viscous resistance may be non-Newtonian. This would be

expected to occur at high rates of deformation.

Since both relaxation times are temperature dependent, we would expect the critical velocity of flow to depend on the temperature. Thus for any given temperature, two limiting velocities should be found, one corresponding to λ_2 and one to λ_3.

The above treatment is a simplified approach, and to represent the behaviour of real materials over a wide range of stress and strain rates each of the relaxation times mentioned must be replaced by a spectrum of such times, and the mechanical model would then consist of a number of elements in series. The critical velocities mentioned would not then be sharp, but would consist of a finite band.

CHAPTER 3.

DEFORMATION OF METALS

3.1 THE STRESS-STRAIN CURVE

The true stress-strain curve of a polycrystalline metal under simple loading is shown in fig. (3.1). That is from a tensile test, the mean stress acting over the current cross-sectional area is plotted against the total strain.

At first the strain is proportional to the stress up to the elastic limit B where the stress is equal to the yield stress Y_o. The slope of the line OA where Hookes law is obeyed gives Young's Modulus of the material. Above the elastic limit B the strain increases with the stress in a non-reversible manner. Due to work-hardening the stress required to produce further strain increases as shown by the part BD of the curve. At any point D if the stress is removed the specimen contracts elastically to O'. On reapplying the stress the deformation will be elastic along O'D until at D plastic deformation again occurs. The yield point D is now much higher than the initial yield stress Y_o, and the bend over near D is much sharper.

Thus if the stress-strain curve of a specimen which has already undergone considerable plastic deformation is plotted, it has the form shown in fig. (3.2) where the yield stress varies little with the strain. Thus a highly work-hardened metal has the properties of what may be called an ideal
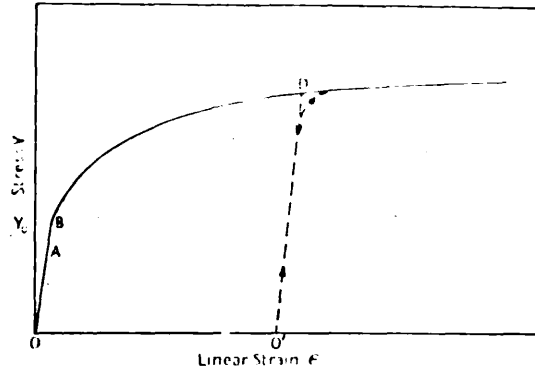
Fi.. **3.1.**True stress-strain curve under tension for a metal which work-hardens as a result of deformation. OA is the elastic region, and B marks the elastic limit or yield stress Y_0 at which plastic deformation commences. As deformation proceeds there is a steady increase in the stress at which plastic deformation occurs. At the point D if the stress is removed, the stress-strain curve follows the reversible path DO'.

FIG. 3.1
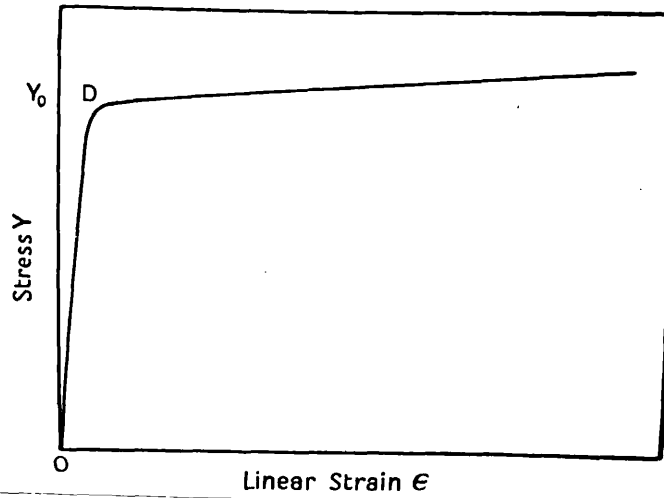
FIG. 3.2

plastic material, namely that of constant yield stress.

3.2 DEFORMATION UNDER COMBINED STRESSES

When the surface of a metal is deformed by a sphere, the stresses are not simply compressive or tensile, so we must consider plastic deformation by combined stresses.

Experimentally it is found that a moderate hydrostatic pressure does not produce yielding. Thus under the influence of combined stresses, only the non-hydrostatic part will cause plastic flow. Suppose a metal is subjected to principal (orthogonal) stresses p_1, p_2, p_3. These are equivalent to the sum of a hydrostatic component $\frac{1}{3}(p_1 + p_2 + p_3)$ and reduced stresses,

$$p_1 - \frac{1}{3}(p_1 + p_2 + p_3), \quad p_2 - \frac{1}{3}(p_1 + p_2 + p_3) \text{ and } p_3 - \frac{1}{3}(p_1 + p_2 + p_3)$$

Only the reduced stresses cause plastic deformation and experimentally it is found that they do so when the sum of their squares is constant.

i.e. $\frac{1}{3}\left[(p_1 - p_2)^2 + (p_2 - p_3)^2 + (p_3 - p_1)^2\right]$ = a constant

For uniaxial tension (or compression) $p_2 = p_3 = 0$ and the yield stress $= p_1 = Y$

Hence the value of the constant $= \frac{2}{3}Y^2$

Thus the equation becomes,

$$(p_1 - p_2)^2 + (p_2 - p_3)^2 + (p_3 - p_1)^2 = 2Y^2$$

This equation first derived by Huber (1904) and independently by von Mises (1913) is known as the Huber-Mises criterion of plasticity and is supported by much experimental evidence

(Nadai 1931). It was shown by Hencky (1923) that the equation has a definite physical meaning. The left hand side of the equation represents the stored elastic energy.

An alternative criterion was proposed by Tresca (1864) and revived by Mohr (1900). This assumed that yielding occurs when the maximum shear stress reaches a certain critical value. For principal stresses p_1, p_2 and p_3 the shear stresses are, $\frac{1}{2}(p_1-p_2)$, $\frac{1}{2}(p_2-p_3)$ and $\frac{1}{2}(p_3-p_1)$.

If $p_1 > p_2 > p_3$ the maximum shear stress is $\frac{1}{2}(p_1-p_3)$, and it is this parameter which determines the onset of plastic flow. In the case of a uniaxial tension $p_2 = p_3 = 0$, then the shear stress $= \frac{1}{2}p = \frac{1}{2}Y$.

Thus the Tresca-Mohr criterion is $p_1-p_3 = Y$ when $p_1 > p_2 > p_3$. If two of the principal stresses are equal the two criteria are the same. In the case of plane strain $p_3 = 0$, the Huber Mises criterion reduces to $p_1-p_3 = 2/\sqrt{3}Y$ which is identical with the Tresca criterion except for the value of the constant.

A further criterion due to Haar and von Karman (1909) assumes that two of the principal stresses are equal and finds that as a criterion for plasticity,

$$p_1-p_2 = Y \qquad \text{when } p_2 = p_3.$$

There is no physical basis for this assumption but the criterion is useful for solving certain otherwise intractable problems.

TWO-DIMENSIONAL PLASTIC FLOW

The only problems of plastic indentation which have been rigourously solved are those involving two-dimensional deformation. The starting point is the assumption that plastic flow occurs when the Huber-Mises criterion is satisfied, which is equivalent to saying that it occurs when the maximum shear stress reaches a critical value k, where 2k = 1.15Y. The principal stresses P and Q can be combined to produce a hydrostatic component p and a shear stress k, where p = ½(P+Q) and k = ½(P-Q). This is shown in fig. (3.3). Thus when plastic deformation occurs, the stresses at any point may be expressed in terms of a shear stress k, and a hydrostatic pressure p; k is constant, but p varies from point to point. The lines of maximum shear stress k are called slip (or shear) lines, and are two sets of orthogonal curves. Then if the hydrostatic pressure at any point is known we can deduce the principal stresses, since

$$P = p+k \quad \text{and} \quad Q = p-k.$$

If the slip lines are straight, p is constant, but if the slip line turns through an angle ϕ relative to any fixed direction, then $p \pm 2k\phi$ = a constant along a line, the value of the constant being obtained from the boundary conditions.

The slip-line theory can be applied to solve problems, such as the magnitude of the stress under an indentor, the constants are determined from the conditions at the free surface outside the indented area.
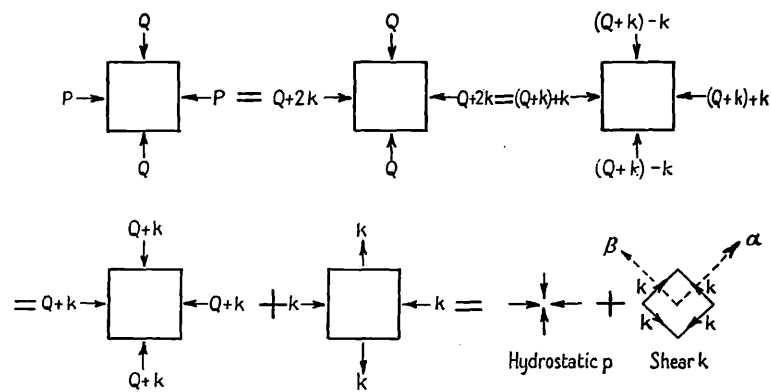
Fig. 3.3 Diagram showing that for two-dimensional stress, the principal stresses P and Q may be replaced by a hydrostatic pressure p and a maximum shear stress s, where $p = Q+k = P-k = \frac{1}{2}(P+Q)$ and $s = k$.

Fig. 3. 3

CHAPTER 4

PROPOGATION OF TRANSIENT DISTURBANCES

4.1 INTRODUCTION

The action of a suddenly applied load is not instantaneously transmitted to all parts of the loaded body. Initially the remote portions of the body remain undisturbed. Deformations and stresses produced by the load move through the body in the form of waves which travel at a finite velocity. When these waves strike the boundaries of the body they may be wholly or partially transmitted, or reflected back into the body where they may reverberate back and forth. By superposition of these radiated and reflected waves the stress and motion of all parts of the body are gradually, and in general, discontinuously brought up to the values ordinarily assumed when the bodies are considered "rigid". When the time of application of the force is long this adjustment is easily made, but in the case of impact when the time element is short the process must be studied in detail.

Various types of stress wave can be produced, longitudinal, transverse and surface waves. In addition these can be either elastic or plastic. These are discussed by Timoshenko (1951), Donnel (1930), Kolsky (1953) and Broberg (1956). The simple case of longitudinal wave transmission in a rod will be discussed with the extension to the plastic case. This appears to be the type of system which has been

considered most fully, particularly for the plastic case, both theoretically and experimentally. A large amount of work has been done however on the propogation of elastic waves in infinite solids from the point of view of geophysical prospecting.

Although the idea of the interaction of stress waves is important for an understanding of impact phenomena, it is only in certain very simple cases that the process can be analysed completely. In particular the interpretation is difficult when the stress pulse is longer than the dimensions of the body.

4.2 LONGITUDINAL WAVES IN RODS.

The equation of motion can be easily derived if plane cross-sections of the rod are considered to remain plane and the stress over them uniform. Considering the forces on a small element of the rod of length x we obtain the equation of motion

$$\frac{\partial^2 u}{\partial x^2} = \frac{1}{E/\rho} \frac{\partial^2 u}{\partial t^2}$$

where u is the displacement of the element. Thus longitudinal waves are propogated with velocity $\sqrt{E/\rho}$

The solution of this equation is

$$u = f(C_o t - x) + F(C_o t + x)$$

where f corresponds to a wave travelling in the direction of x increasing, and F to x decreasing.

Consider the solution $u = F(C_o t + x)$

differentiating with respect to x we have

$$\frac{\partial u}{\partial x} = F'(C_o t + x)$$

and with respect to t

$$\frac{\partial u}{\partial t} = C_o F'(C_o t + x)$$

Hence $\dfrac{\partial u}{\partial t} = C_o \dfrac{\partial u}{\partial x} = \dfrac{C \sigma}{E}$ since $\dfrac{\partial u}{\partial x} = \dfrac{\sigma}{E}$

where σ = the stress.

Hence $\qquad \sigma = \dfrac{E}{C_o}\dfrac{\partial u}{\partial t} = \rho C_o \dfrac{\partial u}{\partial t} = \rho C_o v$

$\dfrac{\partial u}{\partial t}$ is the particle velocity = v.   Since v is proportional to σ it will be negative for a tension wave.

4.3 REFLECTION OF WAVES.

By applying the appropriate boundary conditions we can discuss the reflection of the pulse at the end of the bar. At the free end of a bar the stress must be zero.

Consider the compression and tension waves moving together as shown, fig. 4.1. Where the two waves meet the tension and compression annul oneanother and the stress will be zero. The particle velocities will however be 2v. After passing, the waves return to their initial shape. The mid-point of the crossover region where the stress is zero may be compared with the free end of the bar. Thus from the figure it can be seen that at a free end a compression wave is reflected as a tensile wave and vice-versa.

When two similar waves are superimposed the stress will be doubled and the velocity zero. Thus the mid- point of
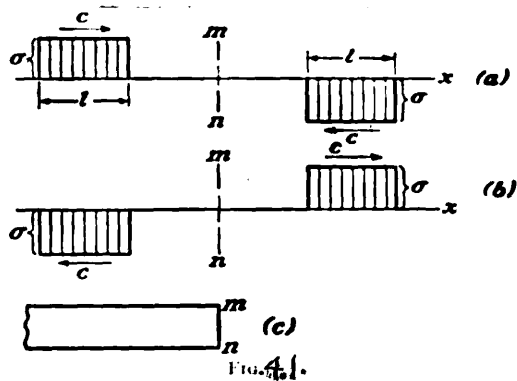
Fig.4.1.

FIG. 4.1
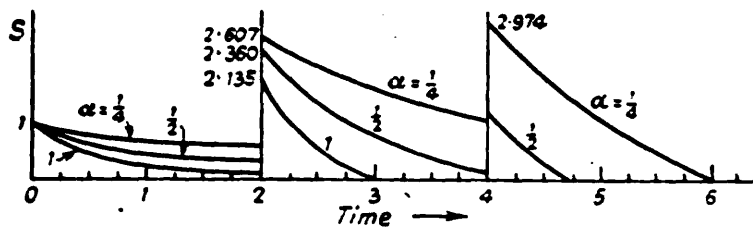
FIG. 4.2.—The sequence of stresses with time at the point of contact in Boussinesq's theoretical treatment of impact.[14]

FIG. 4.2

the crossover region can be compared to a fixed end which must have zero velocity. Hence it can be seen that a wave will be reflected from a fixed end unchanged.

4.4 IMPACT OF RODS.

If two equal rods of the same material strike each other longitudinally with the same velocity v, the plane of contact will not move during the impact (assuming that contact takes place over the whole area of the bars at the same instant) and two identical compression waves start to travel along both bars with equal velocities c. These will be reflected at the free ends as tension waves and after a time 21/c they will reach the plane of contact and the bars will separate with velocity v. The compressive stress is equal to $v\rho c = v\sqrt{E\rho}$

4.5 LONGITUDINAL IMPACT BY A FINITE MASS

If the mass is rigid but of a finite magnitude M, then the compression in the rod at the end in contact with it will decelerate it, and its velocity (and hence the velocity of particles in the rod at this point) will gradually decrease. Hence the compressive stress in the rod will also decrease from its initial value $\sigma_0 = v\sqrt{E\rho}$ The equation of motion can be written

$$M \frac{dv}{dt} + \sigma = 0$$

where M is the mass of the body per unit cross section of the bar.

Hence
$$\frac{M}{\sqrt{E\rho}} \frac{d\sigma}{dt} + \sigma = 0$$

$$\sigma = \sigma_0 e^{-t\sqrt{E\rho}/M}$$

Thus the stress decreases exponentially from its initial value until the time $t = 2l/c$ when the reflected wave arrives back at the plane of contact. If the end of the bar is free the reflected tensile wave will increase the particle velocity in the bar and contact will cease. On the other hand at a fixed end, the reflected wave is compressional and if the mass M is large will be reflected also at the plane of contact and will thus contribute to the stress already existing there. In this way the stress at the contact area can build up in a series of steps. The final stress and the time of contact depend on the ratio (α) of the mass of the striker to the mass of the rod. Fig. (4.2).

In the above treatment the elastic properties of the striker have not been taken into account. These can be allowed for by assuming that on impact the plane of contact moves so that the ~~compressions~~ pressures of the waves in both bodies are the same. Thus the expression for the initial stress becomes,

$$\sigma_0 = v \frac{\sqrt{E_1\rho_1 E_2\rho_2}}{\sqrt{E_1\rho_1} + \sqrt{E_2\rho_2}}$$

Boussinesq (1893) extended the above ideas to consider the minimum striking velocity required to damage a plate and obtained essentially the same equation except for a multiplying factor equal to 1.06.

4.6 PROPOGATION OF PLASTIC WAVES

The propogation of a plastic disturbance where the stress-strain curve is non-linear, was first considered by Donnell (1930), using a graphical method. Theories were developed independently by Taylor (1946), von Karman (1950) and Rakhmalutin (1945). They considered the case of a thin wire the end of which is suddenly given a velocity V for a time t. They assumed that the velocity of propogation of a particular strain depends upon the slope of the engineering stress-strain curve, fig.4.3, at that value of the strain. Thus the equation of motion becomes,

$$\frac{\partial \sigma}{\partial \epsilon} \cdot \frac{\partial^2 u}{\partial x^2} = \rho \frac{\partial^2 u}{\partial t^2}$$

and the velocity of the plastic wave for a given strain is given by

$$\sqrt{\frac{\partial \sigma}{\partial \epsilon} / \rho}$$

The end of the bar was moved with velocity V and it can be shown that

$$V = \int_{c}^{\epsilon} V(\epsilon) d\epsilon$$

When the strain reaches the value ϵ_m corresponding to the ultimate strength of the material, the slope of the engineering tensile stress-strain curve $d\sigma/d\epsilon$, becomes zero. Thus a critical impact velocity occurs, above which fracture would be expected near the point of impact since the stress cannot be propogated.

This has been found experimentally for metals Clark and Wood (1950) Maxwell and Harrington (1952) discuss its
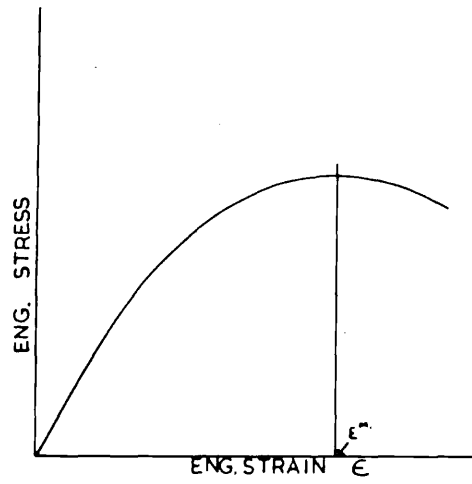
FIG. 4. 3
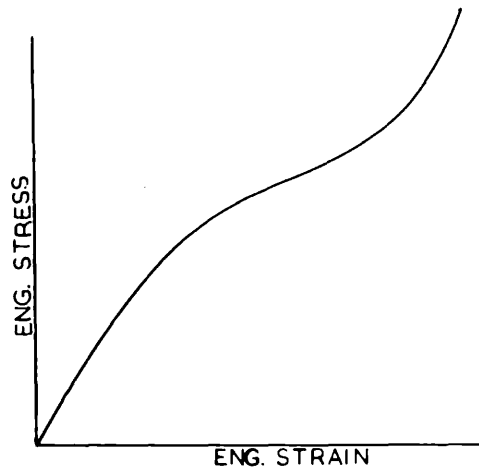
FIG. 4. 4

applicability to polymers.

The above discussion applies to tension impact.   In
compression the stress-strain curve can be concave upwards
fig. 4.4 and a shock wave may be set up.

White and Griffis (1948) have analysed the modes of
propogation of a uniaxial compression wave in a bar and show
that a number of different kinds of behaviour are possible,
depending on the impact velocity.   These are as follows:

(1)   Elastic impact.   Impact stress proportional to the
                                    impact velocity.

(2)   Normal Plastic Impact.   This is similab to the
                                    tension impact discussed.

(3)   Normal Shock-Wave Behaviour.   Stress and strain
            propogate as a shock wave with very large stress-
            strain gradients similarly to shock waves in gases.

(4)   Flowing Deformation.   The impact is too severe for
            for the material to retain coherency, and there-
            fore it flows toward and along the surface of the
            target.

(5)   Supersonic Impact.   The impact velocity exceeds the
            speed of an elastic wave in the medium, and the
            material behaves like an incompressible fluid.

4.7   FRACTURE DUE TO SUPERPOSITION OF STRESS WAVES
    Experiments in which the time of loading is very short,
so that the length of the stress pulse is short compared with
the dimensions of the specimen, can be analysed by considering

the superposition of the initial and reflected waves from the bottom and sides of the specimen. Scabbing due to an explosive charge on a thin plate is a typical example. Many experiments have been performed on "Perspex" with small charges. Kolsky and Shearman (1949), Kolsky and Christie (1952) explained the fracture pattern in terms of the reflection and superpostion of stress pulses. It is noticeable in this type of experiment that since the crack velocity is considerably less than the stress pulse velocity, the cracks do not have time to grow before the stress is removed and thus isolated cracked regions can occur.

Analysis of the intermediate type of experiment where the pulse length is long compared with the specimen size, is considerably more complicated than either the above case or the other extreme where the pulse is so long that the Hertz "static" approach is strictly valid. This is the type which occurs however in the velocity range considered here. Fortunately the effect of stress wave interactions is reduced considerably in the specimen at any rate, as we have the case of a spherical wave propogated in a medium with plane boundaries. Thus the stress in the wave front falls off as 1/R and we have no focussing effects. When considering spheres however, although we have spherical waves, focussing effects will occur on reflection at the curved surface. Since the reflected waves will be tensile, this effect can cause a considerable reduction in pressure at the centre of

of the contact area in the case of a material which flows on impact since the surface of contact will be moving into the material and will approach the region of reduced pressure. A detailed analysis of the effect would be difficult however in view of the spherical nature of the waves and changes in the boundary conditions during the course of the impact.

CHAPTER 5.

HERTZ THEORY OF IMPACT

5.1 HERTZ EQUATIONS

Hertz (1881) first considered the static case of two curved bodies in contact. He obtained the following relation between the force P and the distance α through which the bodies are pressed together,

$$P = k\alpha^{3/2}$$

where k is a constant depending on the geometry of the bodies in the region of contact and their elastic constants.

To extend the above idea to the case of impact we determine P in terms of the rate of change of momentum of the impacting bodies.

For the case of a sphere of radius R striking a plane normally with velocity v the equations for the maximum value P_m of the total force developed during impact is

$$P_m = \frac{4}{3}(1.25\pi\rho_1)^{3/5}\left(\frac{E_1 E_2}{E_2(1-\sigma_1^2) + E_1(1-\sigma_2^2)}\right)^{2/5} R^2 v^{6/5}$$

where $E_1, E_2, \sigma_1, \sigma_2$ are respectively the Young's Moduli and Poisson's ratios of the sphere and the solid. ρ_1 the density of the sphere.

At maximum compression the radius, a_m of the circle of contact is,

$$a_m = \left\{1.25\pi\rho_1\left(\frac{1-\sigma_1^2}{E_1} + \frac{1-\sigma_2^2}{E_2}\right)\right\}^{1/5} R v^{2/5}$$

The mean normal pressure p_m at maximum compression is

$$p_m = \frac{P_m}{\pi a_m^2} = \frac{4}{3\pi}(1.25\pi\rho)^{1/5}\left(\frac{E_1 E_2}{E_2(1-\sigma_1^2) + E_1(1-\sigma_2^2)}\right)^{4/5} v^{2/5}$$

The pressure across the circle of contact is not uniform but at any point distance x from the centre of the indentation has the value

$$p = p_0(1 - x^2/a^2)^{1/2}$$

where p_0 is the pressure at the centre of the circle of contact fig. 5.1.

It follows that

$$p_0 = \frac{3}{2} p_m$$

5.2 YIELD POINT

In the case of metals if we apply the Tresca-Mohr, or Huber-Mises criterion, it is found that the condition for plasticity is first reached at a point below the actual surface of contact. This was shown by Davies (1949), fig. 5.2. The maximum value of the shear stress occurs at a point about 0.5a below the circle of contact and is equal to $0.47p_m$ when Poisson's ratio is taken as 0.3, as for most metals. The maximum tensile stress occurs at the edge of the circle of contact and is given by,

The Maximum Tensile Stress $= \frac{(1 - 2\sigma)}{3} p_0$

If $\sigma = 0.35$ as in the case of Perspex, the Maximum Tensile Stress $= 0.1 p_0$.
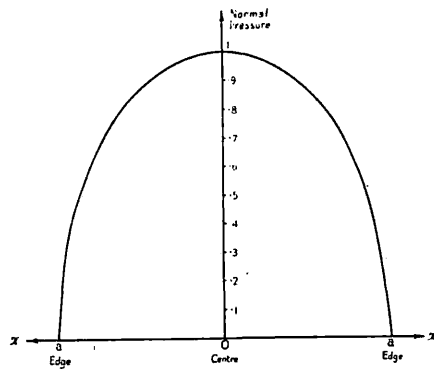
FIG. 5.1. Pressure distribution over circle of contact when a flat
surface is deformed elastically by a sphere.

$$\text{FIG. 5.1}$$
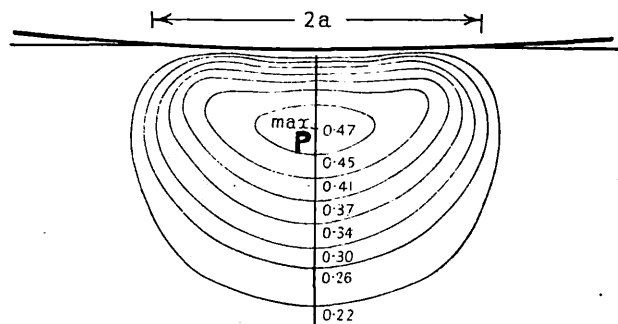
FIG. 5.2. Elastic deformation of a flat surface by a sphere, showing the maxi-
mum shear stress in the bulk of material below the deformed surface (Davies,
1949). The maximum shear stress occurs below the centre of the circle of
contact and has a value of about $0.47P_m$, where P_m is the mean pressure.
Plastic deformation first occurs at this point when the shear stress $= \frac{1}{2}Y$, i.e.
when $P_m \approx 1.1Y$, where Y is the yield stress of the metal.

$$\text{FIG. 5.2}$$

5.3 VALIDITY OF THEORY

The validity of applying the statical Hertz theory to a
dynamic case depends on the velocity of impact and the geometry
of the impacting bodies.   In general for moderate velocities
and small curved bodies the theory is applicable.   Hertz
states: "The time of impact is small in absolute value; yet
it is large compared with the time taken by elastic waves to
traverse distances of the order of magnitude of that part of
their surfaces which is common to the two bodies when in con-
tact i.e. the surface of impact.   Thus the state near the
point of impact is nearly the same as the state of equilibrium
produced by the total pressure existing at any instant between
the two bodies,supposing it to act for a long time.   Thus we
can apply the static theory for the relation between force
and distance of approach and use the equations of motion of
elastic solids.   If we assume that the time of impact is also
large compared with the time taken by elastic waves to traverse
the solids from end to end, then the bodies, except those
parts very near the point of impact, behave as rigid bodies."

Rayleigh (1906) considered the energy loss due to
vibration, in the impact of two spheres and derived a
relation for the loss in terms of the velocity of impact v
and the wave velocity in the medium.   If this loss is small
the Hertz theory would be expected to hold.   The relation

derived was $R = \dfrac{\text{Kinetic Energy of the vibration}}{\text{Total Kinetic Energy before collision}}$

where the value of $R = \dfrac{1}{50} \dfrac{v}{\sqrt{E/\rho}}$.

Thus the loss is very small except at very high velocities.

S.C. Hunter (1957) discusses the validity of the Hertz theory and states that a relation $\left(\dfrac{v}{c}\right)^{1/5} \ll 1$ is obtained. This is considerably more restrictive than the Rayleigh criterion. He does however state that when a collision takes place between a small and a massive body, the criterion of the time of transit of the elastic waves need only be applied to the small body. This is in agreement with the conclusions of the present author. Indeed if a small sphere is in collision with an infinite solid, it is difficult to see how any other idea can be valid. If the two solids are of a similar size however the case is quite different, in respect to the time of contact, but not necessarily so when considering the stresses set up in the neighbourhood of the area of contact.

Wagstaff (1924) and Prowse (1936) studied the impact of metal bars with spherical ends to verify the validity of the St. Venant and the Hertz theory. Crook (1952) has determined the force-time curve for impact between two cylinders using a piezo-electric crystal. His results are in agreement with the theoretical curve obtained by numerical integration, fig. 5.3. Since he mounted one specimen at the end of a long rod, the results show that the Hertz theory can be applied to the case where the time taken by the elastic wave to traverse
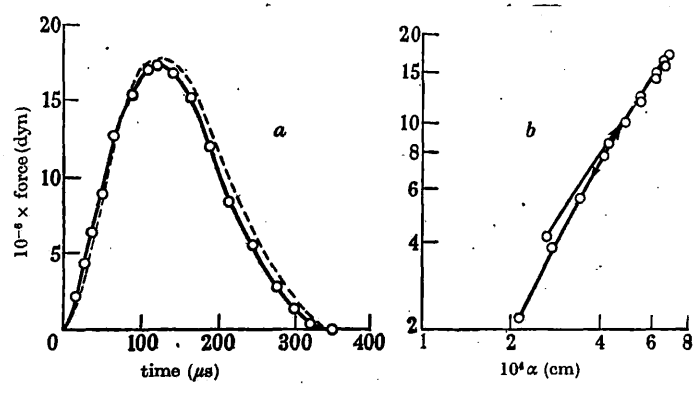
FIGURE 5.3. Impact between 1 in. (2·54 cm) diameter copper cylinders at 10 cm s⁻¹ velocity of approach. (a) Force-time curves. O, experimental; ----, theoretical. (b) Indicator diagram (log-log plot).

F₁ɢ. 5. 3
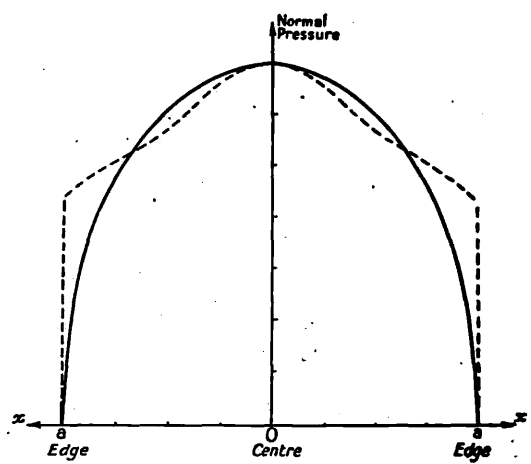
Fɪɢ. 5.4. Pressure distribution over circle of contact for a metal deformed by a spherical indenter. Full line, elastic deformation (Hertz); broken line, plastic deformation (Ishlinsky).

F₁ɢ. 5. 4
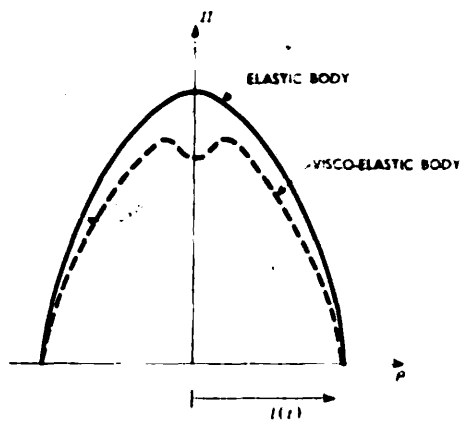
Fig.5.5. Contact Pressure Distribution.

F₁ɢ. 5. 5

one of the bodies may be long compared with the time of impact, as stated above from a general argument.

In discussing the high speed impact of steel balls on glass Haward (1945) states that in high velocity fracture, high stresses are generated at the time of initial contact before the glass has started to bend appreciably. Thus with thick plates and small balls at a high velocity it is possible for the glass to break first under the Hertzian forces round the circle of contact.

5.4 IMPACTS PRODUCING PLASTIC DEFORMATION

The result obtained by Davies refers to the onset of plastic deformation in the metal. When the velocity of impact is increased, the amount of plastic deformation will increase until the whole of the material around the indentation is in a state of plasticity. The theoretical analysis cannot be carried out rigorously for the axially symmetrical case. Ishlinsky (1944) has however obtained a solution for the pressure distribution using the Haar-Karman criterion of plasticity. Although the assumptions made are not strictly valid, the result may be considered a good approximation, and is in agreement with experimental data. The pressure distribution over the fully plastic indentation can be compared with that for elastic deformation in fig. 5.4. The distributions are similar, which accounts for the spherical nature of indentations after elastic recovery has occurred.

5.5 INTRINSIC INELASTICITY OF PLATES

Zener (1941) has discussed the impact of a sphere on a plate with respect to the intrinsic inelasticity of the plate. He solves simultaneously the equations of motion of the sphere and the plate. The reaction of the plate on the sphere is given by the Hertz equation.

He obtains an inelasticity parameter λ, which falls to zero for fully elastic impacts, rising to unity when the coefficient of restitution is 0.2.

$$\lambda = \frac{\pi^{3/5}}{3^{1/2}} \left(\frac{R}{2h}\right)^2 \left(\frac{v_0}{c}\right)^{1/5} \left(\frac{\rho_1}{\rho_2}\right)^{3/5} \left(\frac{E_1'}{E_1' + E_2'}\right)^{2/5}$$

where R = radius of the sphere, h = thickness of the plate,

v_0 = impact velocity $\qquad c = \left(E_2'/\rho_2\right)^{1/2}$

ρ_1, ρ_2 = densities of ball and plate

$$E_1' = \frac{E_1}{1-\sigma_1^2} \qquad\qquad E_2' = \frac{E_1}{1-\sigma_2^2}$$

For velocities where $v_0 < c$, the main factor determining the value of λ is the $(R/2h)^2$ term.

A value of λ was calculated for the case of a steel ball on "Perspex", for v = 400 ft/sec., R = 0.1 ins. and h = 0.25 ins. giving λ = 0.04. This small value of λ implies that the motion may be considered to be elastic, and that losses due to vibration of the plate are negligible.

5.6 VISCO-ELASTIC MATERIALS

Lee (1957) has applied the Hertz theory to the case of contact between a rigid sphere and a visco-elastic solid.

He considers a Maxwell body and shows that the qualitative
influence of visco-elasticity on the contact pressure
distribution curve is as shown in fig. 5.5. The central dip
represents the influence of the contact pressure which was
concentrated over a smaller area in the initial stages of
deformation. The magnitude of this effect will of course
depend on the relaxation time of the material and the time
of contact.

CHAPTER 6

LIQUID DROP IMPACT

6.1 INTRODUCTION

The first investigations into liquid drop impact were made by those interested in the damage caused in steam turbines by the water drops present in wet steam. The phenomenon is now receiving intensive study, since serious damage results from rain drop impact on the leading edge of aircraft flying at high speed.

6.2 IMPACT PRESSURE

An expression can be obtained for the thrust exerted by a liquid striking a surface in a simple manner by considering the rate of transfer of momentum to the surface, assuming the liquid to be a perfect i.e. incompressible fluid. This method has been used by Hopkinson (1914) and Davies (1948) to evaluate the force exerted by a lead pellet striking the end of a pressure bar at a velocity of the order of 1,000 ft/sec., assuming that at this velocity the lead behaves as a fluid. They obtained fairly good agreement with the calculated pressure.

Consider a cylinder of the liquid of area A striking the surface with velocity v. If the density of the liquid is ρ, then the momentum transfer/ sec. = Force = $\rho vA.v = \rho Av^2$. If the area of the surface struck (i.e. the end of the pressure bar) is A', then the pressure p' at a point inside the surface

is given by $\qquad p' = \left(\rho \dfrac{A}{A'}\right) v^2$

This is the pressure measured experimentally with the pressure bar. Better agreement was obtained by imposing a correction term to allow for the finite yield stress of the bullet, though this was only of the order of a few per cent. Thus at this velocity the assumption that the lead is an incompressible fluid appears to be justified.

If we regard each particle of the liquid as being brought right up to the surface and then stopped, the average pressure will be given by $p = \rho v^2$. No indication of the distribution of the pressure can be given however.

6.3 COMPRESSIBLE FLUID

If the fluid is regarded as compressible a wave motion will be set up on impact, analogous in the uniaxial case to the "water hammer " phenomena occurring in a pipe due to the sudden closing of a valve, Rich (1951). The wave will travel through the fluid with the velocity of sound c. The rise in pressure at the stoppage, due to the reaction of the wave, can be calculated from the fluid velocity v and the velocity of sound, in a similar manner to that used for determing the stress set up in the longitudinal impact of rods in Chapter 4. Thus the pressure exerted = $p = \rho cv$ where ρ is the density of the liquid. Reflection of the wave can also occur as in longitudinal impact, and if the returning wave is tensile a sudden reduction in pressure can occur when it reaches the

original surface. The above argument neglects any effects due to the elasticity of the pipe containing the liquid. Engel (1955) has extended the above idea to the case of impact between a liquid sphere and a plane surface. It is shown experimentally that the drop retains its shape on collision but has flow properties as well, the liquid which first strikes the surface spreading the greatest distance. She assumed that a compressional wavelet is initiated in the drop at the first instant of impact. This is reinforced at a certain radius by compressional wavelets initiated at a later stage. Thus in this region the rate of change of momentum is a maximum giving rise to a circle of maximum pressure.

This pressure is given by $p = \frac{1}{2}\alpha\rho c v$
where α is a factor due to the flow properties of the drop and will depend on the velocity of impact v. $\alpha = 0.9$ for a velocity of 800 ft./sec. This is the maximum pressure developed initially, no pressure-time curve is obtained.

The diameter of the circle of pressure is equal to,

$$D = 2d \, \bar{v}/c(1 - \bar{v}^2/c^2)^{\frac{1}{2}} \approxeq 2d \, \bar{v}/c \qquad \text{when } \bar{v} \ll c.$$

where $\bar{v} = 2(1-\alpha)v$ i.e. the velocity of the effective striking surface. This diameter is quite small compared with the diameter (d) of the drop i.e. for $v = 1,000$ ft./sec., $c = 5,000$ ft./sec., $\alpha = 0.9$,

$$D/d = 0.1$$

If the diameter of this circle of maximum pressure determined the size of the damage site, for a given drop diameter this

equation would predict that the size should be proportional to the velocity.

6.4 WAVE MOTION IN THE DROP

The spherical compressional waves initiated in the drop will be reflected at the back surface. Because of the curvature there will be a focussing effect. Since the process is very complex due to the many factors involved i.e. spherical wave propogation, changes in the shape of the drop, possibility of shock waves occurring, a detailed analysis would be extremely difficult.

Cole (1948) gives data regarding the variation in the velocity of a shock front as a function of the pressure, for pressures of the order of a few kilobars (1 kilobar = 10^9 dynes/sq.cm).

The estimated pressure occurring in water-drop impact is of the order of 2-3 kilobars at velocities up to 1,000 ft/sec. The percentage increase in velocity of the shock front over the acoustic velocity is about 10%-20%. Thus it seems that the phenomena can be treated in terms of sound wave velocities to a close approximation, since in any case the amplitude of the spherical waves will fall off inversely as the distance from the source.

The compressional wave will be reflected at the free surface of the drop as a wave of rarefaction. When focussing occurs however, a negative pressure could develop as the total

amplitude of the returning waves would be larger than the forward going compressional ones. The water will not withstand any appreciable tension under normal conditions (i.e. with air present) and a region of cavitation may be formed, in any case the pressure will be reduced at the centre of the impact site. The velocity with which the impacting surface moves through the drop will be slow compared with the velocity of sound in the liquid and thus many reflections might occur. This velocity is the difference between the impact velocity v and the velocity imparted to the molecules of the drop by the compressional wave $= \alpha v$. This factor α as mentioned previously will be about 0.9, and will always be less than unity due to the fact that the liquid flows.

Thus the overtake velocity $= (v - \alpha v) = v(1 - \alpha) = 0.1v$. The fact that many reflections can occur as the surface moves through the drop leads to an extremely complicated situation and the Hertzian idea of neglecting the wave motion appears attractive. There is however some experimental evidence which indicates that the wave reflection phenomena are of importance. Engel (1955) measured the average force-time curve for drop impact on a barium-titanate crystal. This was for a velocity of about 27 ft./sec. The total duration of impact was about 1 milli-sec., the time taken for the head of the drop to vanish. The force rose to a peak and fell to a value about 1/10 of the maximum in a time of the order of 10 sec. The diameter of the drop was about 0.6 cms., thus

the time for a sound wave to travel to the free surface of the
drop and back again with a velocity of 500 metres/sec. is of
the same order.   This would explain the sudden drop in the
curve.   It must be noted that only the force is measured and
no real idea of the pressure can be obtained, and also the
impact is on a very small area compared with the total area of
the Piezo-electric crystal and the electric charge produced is
an average effect over the whole area.   Further work on this
aspect appears to be needed.   It would be interesting to
measure the average level of the force maintained over the
whole period of the impact.   This might be equal to the
average force determined from the formula given previously for
an incompressible fluid.   This would explain the discrepancy
between the force-time curve for the water-drop and that for
the lead bullet obtained by the pressure bar method, as the
peaked portion of the portion of the pulse may be lost on
passage down the pressure bar.   There are other factors to be
considered however,   such as the fact that the lead bullet is
flat-ended as opposed to the sphericity of the drop, and that
plastic waves will be generated in the bullet.   These will
move into the bullet as a plastic wave front with large stress,
strain and particle velocity gradients.   The particle velocity
will be reduced to zero eventually by the continued reflection
of elastic waves between the rear end of the bullet and the
plastic wave-front.   Whiffen (1948) states however that at
high velocities the velocity of the plastic wave front

decreases and does not penetrate the projectile appreciably, which thus behaves as a jet of an incompressible fluid. One might expect fluid type wave motion to occur however and it would seem that further work on this subject, particularly measurement of force-time curves, is needed.

6.5 OTHER ESTIMATES OF THE PRESSURE

Some other workers in the field have estimated the pressure under an impacting water drop.

Honegger (1927) derives an expression, using the impulse momentum equation and making certain assumptions to allow for the spherical shape of the drop.

His equation is $p = 4v^2\rho$

Owing to the factor of 4, this equation gives pressures of the right order of magnitude at velocities of 800 ft./sec.

De Haller (1933) used the equation for the impact of elastic bars, mentioned previously.

Vater (1944) considers that an equation of the Hertzian type should be more applicable, and quotes results on steel, copper and aluminium in support of this.

6.6 EXPERIMENTAL WORK

Most of the work reported to date has been performed with various forms of apparatus producing multiple impacts. It is not proposed to discuss these in detail, as the author is considering mainly the subject of single drop impact. When multiple impacts occur other factors are involved, their

relative importance varying with the impact velocity and the material concerned, such as fatigue strength and corrosive effects.

It is apparent from the reported results that as the impact velocity is increased, the mechanical forces assume the most important role. Indeed, at higher velocities (of the order of 2,000 ft./sec.) the damaging effect of the wash may be reduced, the liquid just bouncing backwards off the surface, and the phenomenon will approximate more closely to the impact of a solid sphere.

The types of apparatus used have been,

1. Rotating Arm, Wheel and Jet and Interrupted Jet.

2. Shock Wave Apparatus.

3. Magneto-Striction Oscillator.

A review of this work has been made by Engel (1953). The results show that the amount of erosion varies widely with the material of the specimen. In general the materials can be divided into two groups, the first group consisting of those materials in which apparent damage (i.e. either plastic deformation or cracking) occurs with a single blow. The second group consists of those materials in which the energy content of a single blow will be absorbed elastically. In this case damage will usually start at some pressure-raiser, i.e. a small conical pit on the surface. It is evident that this somewhat arbitrary division depends on the velocity range considered, and at the higher velocities the second group will

cease to exist. When deformation does take place an important factor in the case of a metal will be the work hardening capacity and ability to deform without fracture. Similarly with a plastic material, the amount of elongation at break is important.

6.7 CONCLUSION

No really satisfactory theory for the pressure developed in liquid drop impact appears to have been derived, but considerable progress has been made in understanding the phenomenon.

CHAPTER 7

DESIGN OF GUN AND ANCILLARY EQUIPMENT

7.1 INTRODUCTION

An air gun and associated equipment were designed to fire small projectiles at various controlled velocities, up to about 1,000 ft./sec. The velocity was measured electronically using photo-cells. The procedure for arresting the pellet depended on the type of impact process occurring.

7.2 DESCRIPTION OF APPARATUS

The general arrangement is shown in fig. 7.1. The gun, safety tube and photo-cells etc. are mounted on a framework of "Dexion" Slotted Angle so that they can readily be adjusted and aligned. The electronic timing apparatus is mounted underneath the photo-cells, thus keeping the connections short.

7.3 GUN

The gun consists of a smooth bore barrel, 33 ins. long, screwed into the pressure chamber. This is sealed by a valve mounted on the end of a rod. A piston attached to this rod slides in the adjacent trigger chamber which is sealed off from the pressure chamber by an "O" ring seal mounted on the rod in front of the piston. Since the relative area of this piston is large, a small pressure is sufficient to drive back the piston, this opening the valve. Loading is effected by unscrewing the barrel and inserting the projectile. The bore sizes used have been nominally 11/64 ins., 3/16 ins.,
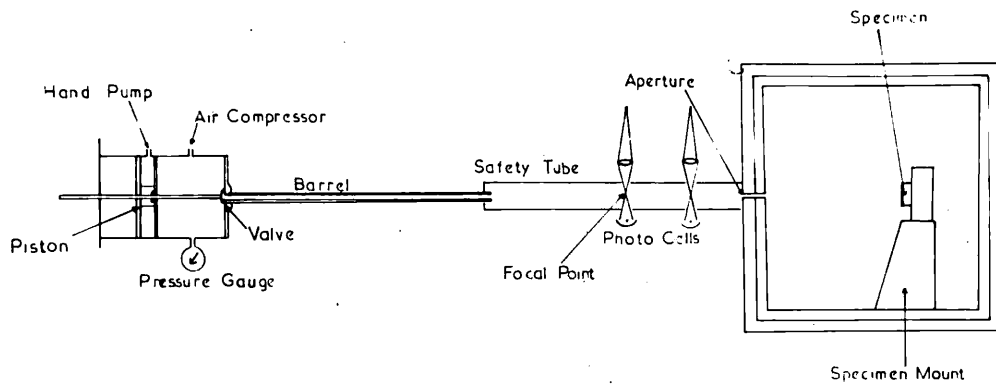
SCHEMATIC ARRANGEMENT OF GUN AND SPECIMEN ENCLOSURE

FIG. 7. 1
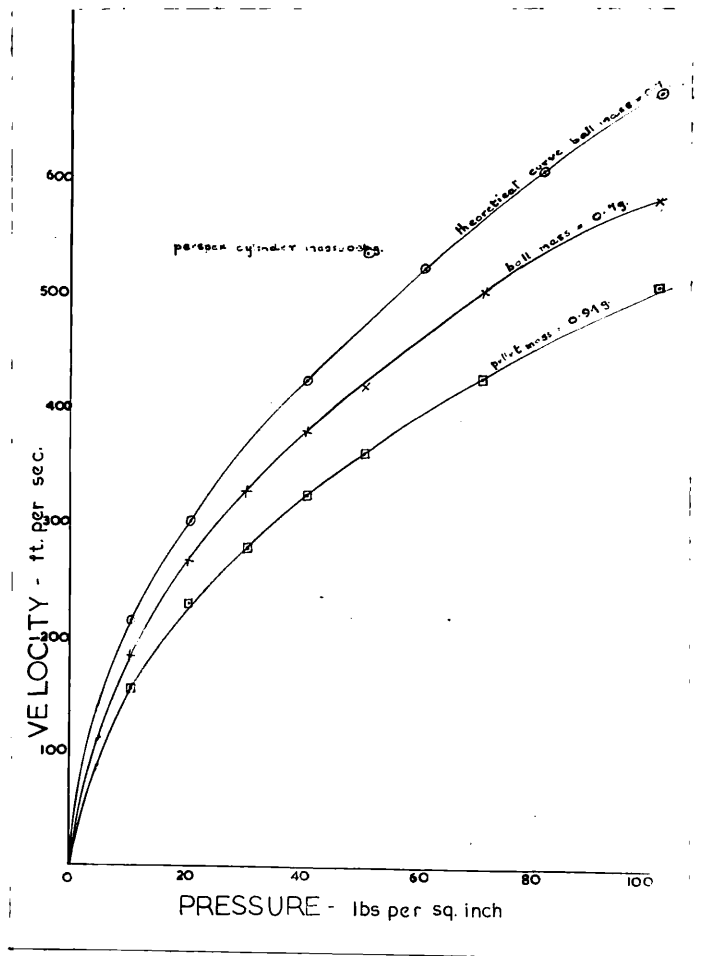
FIG. 7. 2

7/32 ins. and 17/64 ins.

The pressure chamber is pumped up to the required amount indicated by the pressure gauge from a small air compressor with a nominal capacity of 180 lbs. With slight modifications a pressure of 250-300 lbs. was obtained. The triggering pressure is supplied from a bicycle pump or alternatively by a compressed air cylinder.

Pressure-velocity curves are shown in fig 7.2 for a 7/32 ins. ball bearing (mass 0.7 gms.) and a 0.22 in. lead pellet (mass 0.95 gms.) together with the theoretical curve for the ball, obtained by using the approximation of constant pressure, (volume of the pressure chamber = 35 x volume of the barrel). A velocity of 600 ft./sec. is reached with a pressure of 100 lbs./sq.in. These curves were plotted before the compressor was modified. In later experiments firing polythene spheres (mass = 0.05 gm.) a velocity of 1,300 ft./sec. was obtained at a pressure of 300 lbs./sq.in.

Since the mass of gas accelerated is probably larger than the mass of the lightest pellet an increased velocity may be obtained by using a lighter gas (e.g. Hydrogen). This was suggested by D.C. Jenkins (private communication). The working conditions in the laboratory are such however as to make this undesirable, from the danger aspect.

7.4 SAFETY TUBE AND ENCLOSURE

A safety tube is mounted between the muzzle and the specimen enclosure to trap any pellets which might emerge from

the enclosure on rebound. The specimen mount is inclined at about 2° to the normal to prevent repeated impacts occurring due to rebound. This also ensures that pellets do not re-enter the safety tube from the enclosure and possibly trigger the photo-cells. The enclosure, constructed of 1/16 in. Duralumin sheet is fairly large, 2 ft. square, to facilitate adjustments to the specimen. A brass disc, ¼ in. thick is attached to the end of the safety tube, to withstand the impact of the rebounding ball. When using deformable pellets the safety precautions need not be so strict, and the pellet is trapped in a small cardboard box since the specimen must be as close as possible to the photo-cells for the reasons explained in Chapter 12. The arresting technique for the cylindrical specimens is described in Chapter 13.

7.5 PROJECTLIES AND SPECIMENS

Steel ball-bearings of 7/32 in. and 11/64 in. diameter, and ground and polished glass ballotini of 0.218 in. diameter are used as non-deformable projectiles. Polythene pellets and lead shot are used as deformable projectiles. Short cylindrical flat-ended specimens of "Perspex" and Aluminium were fired at water drops. The size of the "Perspex" and Duralumin specimens used is about 1½ ins. square and ½ in. thick.

The details of the various impactors and specimens will be found in the appropriate chapter.

7.6 VELOCITY MEASUREMENT

(a) Electronic Method

The velocity is determined by measuring the time of flight of the projectile between two points. For convenience in measurement and in order to avoid damaging the nose of the projectile, it was decided to use photo-cells for detecting the passage of the bullet, rather than a method such as the breaking of a wire. Another possible detection method which is non-destructive is to use two small coils and detect the change in inductance when the pellet passes through them. This method however will obviously only be suitable for metal specimens.

A Chronotron electronic timer of the current integrator type is used. It has been described by Hitchcox (1956). It consists basically of a trigger circuit, a low-leakage capacitance and a valve-voltmeter. The trigger circuit acts as a high speed switch and allows the timing current to flow only for the duration of the control signal. The timing current is integrated by the condenser, and the voltage across it, proportional to the charge and hence to the time interval to be measured, is read off the valve-voltmeter. The magnitude of the timing current, and hence the useful range of the instrument, is controlled by a resistance network.

The instrument is sensitive to a voltage change of about 1.4 volts, and will measure times down to the order of 1 milli-second, with an accuracy of about 1-2%. The timer

was checked against two other similar instruments before use.

The photo-cells used are of a high output vacuum type P.E.8. illuminated by a 100 watt projection lamp, having a long narrow filament. A reduced image of this filament is produced in the path of the projectile using a F/2 anastigmatic lens of 1.4 ins. focal length. Thus the two triggering positions are located to within about 1 m$_*$m. The distance between these two positions was made 15 cms.

To convert the voltage pulses obtained from the photo-cells when the bullet cuts off the light falling on them to a square wave, and Eccles-Jordan type of circuit is used. The circuit diagram is shown in fig. 7.3. Matched pairs of valves and components are used to ensure balanced triggering. The pulses from the photo-cells are fed into the main circuit through trigger triodes. Advantages of this method are, (a) the triode is normally biased beyond cut-off so that it does not load the circuit and responds to positive voltage pulses, (b) amplification of the pulse. The non-loading is very important when using the bi-stable multivibrator circuit, and in this case the latter condition was necessary as a very stable circuit is used, biased 10 volts below cut-off.

The design of the photo-cell input circuit involves the usual compromise between output and stray capacity effects. The impedance of the photo-cell and grid leak resistance in parallel is of the same order of magnitude as the leakage capacity to earth at the frequency considered. This was
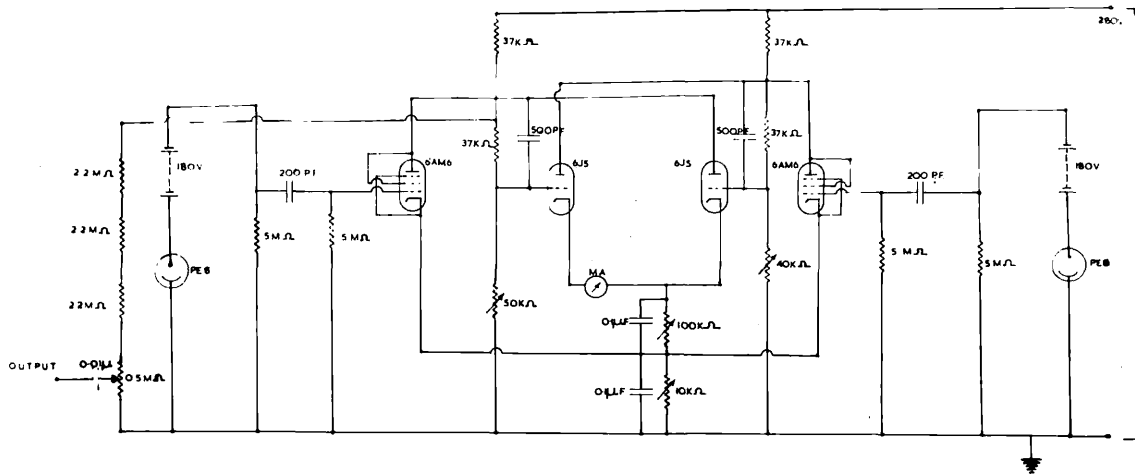
PHOTO-CELL TRIGGER CIRCUIT

FIG. 7.3

THEORETICAL SHAPE

ACTUAL SHAPE
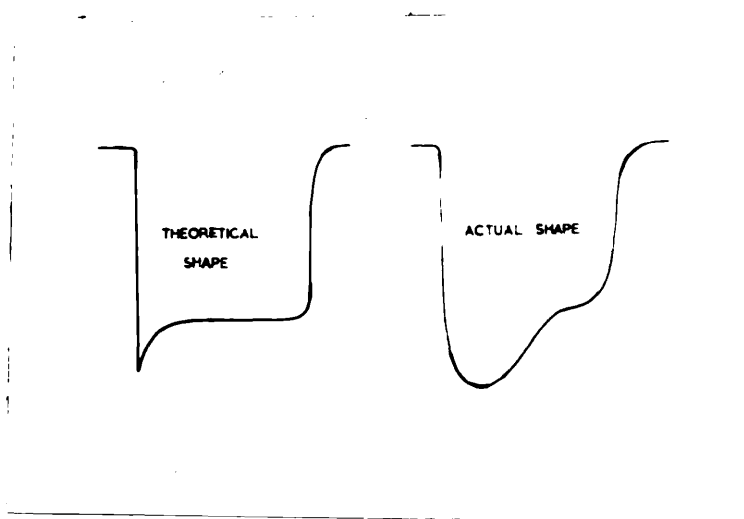
FIG. 7.4

calculated from the duration of cut-off of the photo-cell.
The 200 p.F. coupling condenser is large enough for its
reactance to be small compared with the grid cathode reactance,
but not so large as to cause an increase in the stray capacity.

The output to the timer is taken from an attenuator chain,
inserted to reduce the loading on the circuit and to enable
the output level to be varied.   This is necessary because the
output is not a perfect square wave.   In theory it should be
of the shape shown in fig. 7.4 so that the output required is
such that the timer responds to a point halfway up the curve.
An oscilloscope fitted with a long persistence screen and an
arrangement for obtaining a single sweep was used to try and
detect the shape of the square wave output resulting from the
passage of a pellet.   The intensity of the trace was not
high enough to enable it to be recorded.   In order to con-
tinually trigger the circuit so enabling the time base to be
used, a vibration generator was fitted up with two metal tags
on the vibrating shaft, which alternately cut off the light
from the cells.   The output was observed on the C.R.O. and
the wave form observed is as shown on the diagram at a
vibrator frequency of 300 c./s.   The bulge at the bottom of
the square wave is due to the input pulse from the triode,
as the output is taken from the same point as the input is
fed in.   Its effect is exaggerated here, as the cut-off time
is of the same order as the duration of the square wave,
whereas in the passage of the bullet it is about 1/50 part.

It is also dependent on the time constants of the anode resistance, anode-grid condenser and grid leak circuit, and might be reduced somewhat by using a smaller condenser. This bulge does not matter however provided the timer is operated at the right level of the pulse, i.e. the output to the timer is such that the voltage level at the mean width of the pulse is 1.4 volts.

Since the measured velocity of the gun is consistent within about 2% at a given gauge pressure, a series of times at a constant pressure of 50 lbs/sq.in. were measured for different output levels from the attenuator beginning at the lowest possible level. The curve obtained agrees substantially with that shown on the C.R.O. and thus the output can be set at the required level. Strictly a compensated attenuator should be used, but it is not considered necessary in this case since the pulse width is large.

The "dead time" of the circuit is equal to about 10^{-5} secs. which is much less than the time interval to be measured.

(b) Ballistic Pendulum

As an independent check of the equipment described above, the velocity was measured using a ballistic pendulum. This consisted of a small cardboard box filled with sand and swung as a pendulum length 60 cms. A longer length would be preferable, but space considerations prevented it, this did however reduce the accuracy of the measurement.

Several determinations of the velocity were made and

these all agreed with the value obtained electronically,
within 5%.   This is considered to be a reasonable check of
the photo-cell equipment.

CHAPTER 8

MICROSCOPE TECHNIQUES

8.1 DESCRIPTION OF MICROSCOPE

For most of the interferometric work and photomicrographs a Vickers Projection microscope was used. This is of the inverted type, the specimen being placed above the objective lens. The main collimating system is carried on a movable arm to facilitate the change from transmission to reflection. This is particularly useful in many cases where an obliquely incident beam is required to reveal certain features of interest on the surface, which are not easily detected under normal conditions of illumination. An ordinary bench type microscope fitted with a universal illuminator was also available and used for measurement purposes with a micrometer eyepiece.

The universal illuminator is also fitted to the V.P.M. It incorporates the field condenser and iris, a beam splitter plate of 50% reflectivity and the objective lens. The general arrangement is shown in fig. 8.1. The reflecting plate is mounted on a slide so that it can be moved and replaced by a metal tongue reflector to give/centre pencil illumination.
off

When it is necessary to examine specimens at a low magnification, the universal illuminator can be removed and a long focus lens of up to 5½ ins. focal length inserted. The reflecting plate is then mounted on the microscope stage and
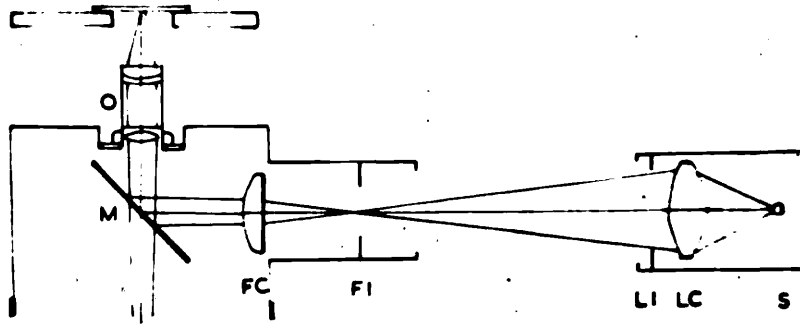
Fig 8.1. V.P.M. optical system: reflection

FIG. 8.1

SPECIMEN

INCIDENT LIGHT

OBJ: CRACKS
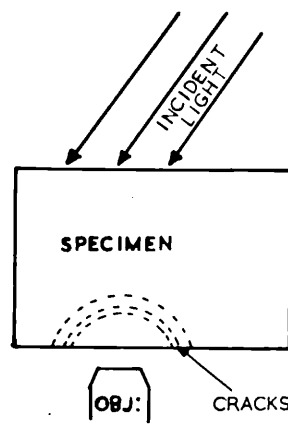
FIG. 8.2

the specimen above that.

This arrangement was used in transmission and reflection and for interferometric study of some of the larger damage . sites. For revealing the surface features of an impact area oblique transmission was useful.

8.2 MEASUREMENT OF CRACK DEPTH

This method was developed by the author to enable the depth of the crazing cracks produced on Perspex by impact to be measured. These occurred in an annular region on the surface. It was necessary to section the specimen at the centre of the annulus, leaving the edge undamaged. This was done by clamping the specimen to another piece of the same material and grinding and polishing the end as one surface. This protected the edge required for examination. The other face was also polished so that it transmitted light.

The specimen was mounted on the microscope stage as shown in fig. 8.2 and illuminated obliquely. Two short rows of cracks will thus be ranged along the lower edge. By adjusting the angle of the incident beam, light will be reflected off the surfaces of the cracks and thus they will appear as bright lines on a dark background when viewed through the microscope. Thus an estimate of the depth of penetration of the cracks can be obtained. The pattern obtained from the cracks produced by a large steel ball is shown in fig. 8.3. This method has also been applied to measurements on impacts
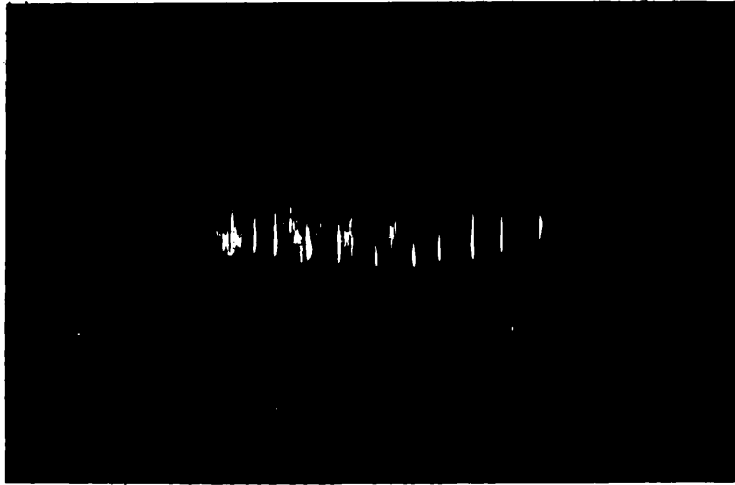
FIG. 8.3   X 100
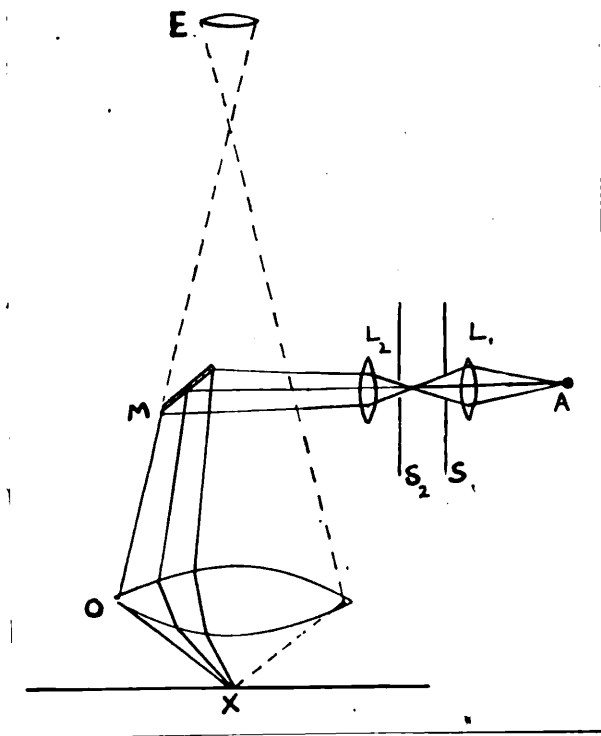
FIG. 8.4

made with polythene spheres.

8.3 THE LIGHT-PROFILE MICROSCOPE

There is a need for a simple method of measuring surface displacements which are too large for interference techniques i.e. where height variations greater than about 1μ occur in a small area, as at a step or with a rough surface. This technique developed by Tolansky (1952) is most suitable for height variation of the order of $1\mu-5\mu$ and is thus very useful.

The method is a development of the light-cut system, (Schmaltz 1936) in which an image of a slit is projected on to a surface by a microscope objective inclined at 45°, and the specularly reflected beam viewed through another objective. The surface profile is then revealed as a displacement of the slit image. The method has several disadvantages. The magnification is limited by the large working distance necessary, and since the profile line is bright on a dark background, location is difficult. An advantage of the method is that the profile displacement/depth ratio is independent of the magnification of the objective; this enables a low mag-nification to be used when scanning a large area.

The light profile system avoids the use of two lenses by using oblique illumination. An off-centre pencil can be obtained using the metal tongue reflector in the universal illuminator mentioned previously. The optical arrangement used is shown in fig. 8.4, where the field iris is in focus

on the surface of the specimen.   A line placed in this plane
will then be imaged on the surface.   This method enables
high magnifications (up to 2,000 x) to be used, so that high
lateral and depth resolutions are obtained.   A disadvantage
is that the angle of the off-centre pencil depends on the
Numerical Aperture of the objective, and thus limits its use
at low magnifications.   A further improvement is to use an
opaque line instead of a slit.   The image then appears as a
dark line on a bright background and hence surface features
can be more easily located.   The line can be either a line
scratched or deposited on glass or the edge of a thin cover
slip.   Since the objective is used to form and view the
image of the line, it is only magnified by a small amount and
thus the precision required is not high.   The optical
requirements to secure good contrast are however quite strin-
gent.   It is essential that a very narrow, preferably slightly
divergent, pencil is incident on the profile line.
Monochromatic light should preferably be used as severe
chromatism can arise from the off-centre pencil.

Although the method is usually used on the V.P.M. where
the necessary adjustments can easily be made, it can also be
used on a bench microscope, provided off-centre pencil
illumination is available.   This is provided by the
universal illuminator which can be obtained as a unit for
bench microscopes.

The relation between the profile magnification M' and

the lateral magnification of the microscope M is

$$M' = M.\frac{\tan i}{\mu}$$

where i is the effective angle of incidence of the pencil and μ the refractive index of the medium between the surface and the objective.

In practise i is not determined, but the instrument is calibrated empirically by measuring the depth of a depression and comparing it with the value obtained interferometrically. The value of $R = \frac{M'}{M}$ obtained for a 6 m.m. flat field objective is 0.90.

8.4 POLARISED LIGHT TECHNIQUES

The V.P.M. is provided with polariser and analyser for observations using polarised light. Quarter-wave plates can also be inserted and orientated sufficiently accurately for qualitative work.

A section was cut from a specimen of Perspex which had been impacted by a polythene sphere. It was examined to see if any residual stresses were observed near the region of impact. No fringes or darkening were observed. Unfortunately this does not prove that no stresses remain since the stress-optical coefficient of Perspex is extremely low. Indeed it is often used for constructional parts in a photo-elastic test where it is necessary for the polarised light to pass through those parts without being affected by the stresses in them. Isochromatic lines can be observed however if the

stress is. large enough. This was shown by observations on
a specimen which had been compressed in a vice, when a large
amount of high elastic deformation would occur.

CHAPTER 9

MULTIPLE-BEAM INTERFEROMETRY

9.1 INTRODUCTION

This technique has been used extensively in the present

work for measurement of the surface distortions produced by

the impact phenomena under investigation.   It was developed

in a series of papers by Tolansky (1944,1945, 1946) and he

has since given a full account of the theory and practise of

the subject (1948, 1955).   A review has also been published

by Kuhn (1951).

Almost all the interferograms were taken using the

reflected system, as it is obviously the only possible method

for studying the surfaces of metals and even with transparent

materials enables surface details to be more easily identified.

A brief review of the theory and practise is given below.

9.2 BASIC THEORY

Fizeau (1862) was the first to use interference methods

for the study of surface contours.   He showed that when

optical interference takes place in a thin transparent wedge

of refractive index μ, straight line fringes occur at wedge

thicknesses t given by

$$n\lambda = 2\mu t \cos \phi$$

where ϕ is the angle of incidence of the light, λ the wave-

length and n the order of interference.   Normally the wedge

must be viewed in reflection, as then the amplitude of the two

interfering beams are similar and the fringe visibility is good.

It can be shown that there will be a Cos^2 intensity distribution along the wedge. Any irregularity in the surface forming the wedge will cause a corresponding displacement of the fringes due to the variation of t. This method is used extensively in the study of surface structure, but the accuracy is limited by the broad maxima and minima of the fringes, inherent in the Cos^2 distribution.

If t is constant, a uniform distribution is seen, the intensity depending on t, but if an extended source is used, interference rings will be formed, Haidinger (1831). In this case ϕ is the variable.

Airy (1831) considered the effect of multiple reflection in a parallel plate system.

The intensity distribution in the transmitted system is the given by

$$I_T = \frac{T^2}{(1-R)^2} \cdot \frac{1}{1 - \frac{4R}{(1-R)^2} \cdot \text{Sin}^2 \frac{\delta}{2}}$$

where T is the transmission and R is the reflection coefficient and $\delta = \frac{2\pi \cdot 2\mu t}{\lambda} \text{Cos} \phi$ is the constant phase lag between successive beams.

It was pointed out by Bouloch (1893) that the effect of increasing the value of R is to sharpen the fringes considerably, fig. 9.1. This effect was used in the Fabry-Perot interferometer. (Fabry and Perot 1897)

R=0·3

R=0·6

R=0·9

FIG. 9. 1

3

2

A

D

θ
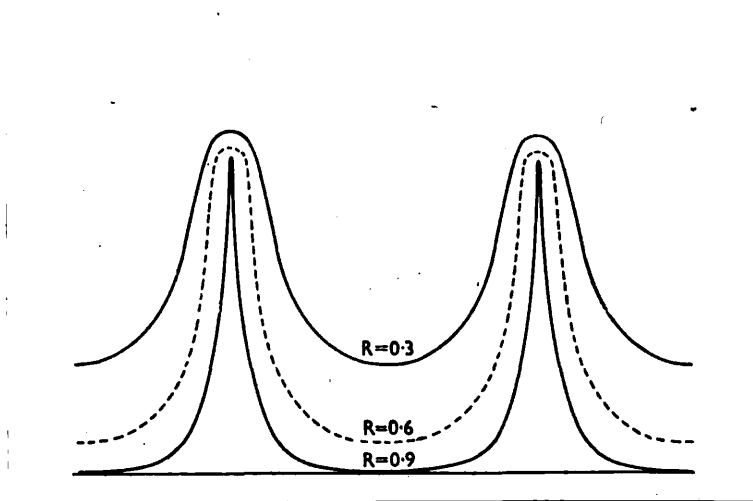
1
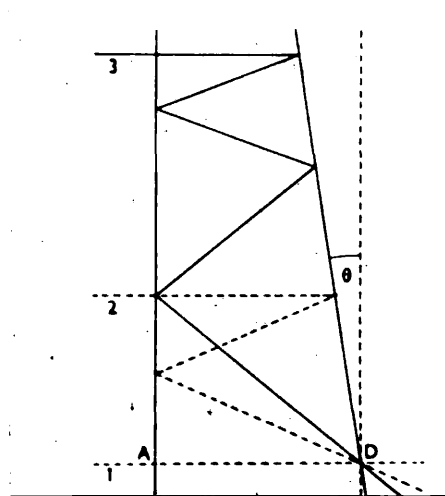
FIG. 9. 2

The first application of this idea to produce sharpened
Fizeau fringes was by Fabry and Buisson (1919). They did
not however analyse the conditions required to produce sharp
wedge fringes. Tolansky (1946) carried out this analysis and
pointed out that though the Airy summation only holds strictly
for a parallel plate, if certain critical conditions are ful-
filled for a doubly silvered wedge, then a close approximation
to the Airy formula applies.

9.3 THE PHASE LAG

The difference between the parallel plate system and the
wedges is that the phase difference between successive beams
is not a constant but a phase lag occurs. Brossel (1947)
gave a general method for calculating this for a wedge of
angle ϵ and obtained the result

$$\text{Phase lag} = \frac{4}{3} n^3 \epsilon^2 t$$

Thus the phase lag increases in each successive beam and
instead of assisting the Airy summation they begin to oppose
it.   This limit occurs when $4/3 \; n^3 \epsilon^2 t$ approaches $\lambda/2$.
Thus it is essential that when high reflectivities are used,
n of the order of 30, that t and ϵ are small. ϵ is limited by
the fact that a certain number of fringes/cm are required.
If there are X fringes/cm. then $\epsilon = \lambda X/2$.   A suitable value
for X is say 50 cm.$^{-1}$, giving 2 fringes/cm. at a magnification
of 25.   Then $\epsilon = X\lambda/2 = 50\lambda/2 = 1.4 \times 10^{-3}$ radians, for
$\lambda = 5461$ A.U. (Hg Green Line).   This is a wedge angle of 5'

Hence if the phase lag for the 30th beam is to be small compared with 2π, say $\pi/4$, then the limiting condition

$$\frac{4\pi n^3 t \epsilon^2}{3\lambda} = \frac{\pi}{4} \quad \text{gives}$$

$$t \simeq 2\times10^{-4} \text{ cm. or } 4\lambda.$$

Thus if these conditions are fulfilled, the intensity distribution given by the Airy summation holds with a slight asymmetry.

9.4 COLLIMATION

Another factor determining the fringe shape is the angle of incidence of the beam.   The effect can be evaluated by considering the change in order due to an angle of incidence ϕ.   If t is small however it is not critical and for t = 0.001 m.m., $\phi = 3^{\circ}$ only gives a change of one two hundreths of an order.   This change gives a method of deciding between hills and valleys, since the broadening will occur on the sides of greater thickness.   To observe appreciable broadening highly convergent light must be used.

Fringe broadening can also arise due to the line width of the source.   Since t is small the chromatic resolution (i.e. analogous to the Fabry-Perot interferometer) is low and for t = 0.001 m.m. a computation shows that the fringe width chromatically is of the order of 50 A.U.   Thus intense sources with broad lines can be used.

9.5 LINEAR DISPLACEMENT OF THE BEAMS

It can be seen in fig. 9.2 that the higher order beams come from regions progressively further away from the first

beam, and the wedge thickness varies over the distance. An essential condition for obtaining a time picture of the surface is that all the beams must come from a region which is well within the resolving limit of the microscope objective. Only then can the fringe shape be said to correspond with the features seen.

The linear separation on the surface of the wedge between the first beam and the nth beam is approximately

$$d = 2n(n+1)t\epsilon = 2n^2 t\epsilon \qquad \text{for large n.}$$

This again is proportional to t and emphasises the need for t to be small.

Thus the upper limit for the numerical aperture, N.A., of the objective used is given by

$$\frac{\lambda}{2N.A.} > 2n^2 t \epsilon$$

The lower limit is set by the requirement that all the effective beams must enter the objective. The successive beams are inclined at angles 4ϵ, 6ϵ, etc. to the original direction, the nth beam subtending an angle $2n\epsilon$. The illumination is not symmetrical since the beams displace in one direction, so that the objective must be able to collect all the beams in its semi angle of collection.

Thus we have $N.A. > \mu \text{Sin } 2n\epsilon$.

9.6 REFLECTED SYSTEM

In this case the first beam has a phase change with respect to the second beam which is quite different from that

between any other two successive beams. This phase change
can affect the fringe shape. The theory has been discussed
by Hamy (1906) and Holden (1949). They showed that the
fringes are usually asymmetrical but the spacing between two
successive minima is as given by the Airy summation. The
symmetry depends on the phase change at the front surface of
the interferometer.

The effect of absorption has not been considered so far,
but it can have a pronounced effect on the reflected system.
If no absorption occurs the minima have zero intensity, but it
rises steeply with increasing absorption.

The factors determining the usefulness of the fringes are
the contrast $(I_{max}-I_{min})$ and the sharpness or inverse half-
width. The former thus depends on the absorption and latter
on the reflectivity. But with silver films the absorption
increases rapidly at high reflectivity which sets a limit to
the sharpness obtainable with the reflected system. An
improvement can be obtained by using a multilayer dielectric
film for the front surface giving a high reflectivity with
low absorption.

Summing up we can say that the conditions to be fulfilled
for the production of sharp multiple beam Fizeau fringes are:
1. The surfaces must be coated with a film of high
reflectivity and low absorption.
2. This film must also reproduce the surface contours
exactly and be of uniform thickness.

3.   Monochromatic light should be used.

4.   The thickness of the wedge must be small to reduce the phase lag.

5.   A parallel beam of light incident normally should be used.

6.   The lateral displacement of the beams should be less than the resolving power of the objective.

7.   The objective aperture should be such as to be able to collect all the effective beams.

The essential factor controlling all these conditions is the wedge gap.

9.7 DIFFRACTION EFFECTS

The possibility that errors in interpretation may occur due to the above effects was pointed out by Brossel (1947) and Wilcock (1951).   If fine structure such as a sharp edge occurs the diffracted light which will be at angles away from the normal will modify the intensity distribution, producing "wings" on the firnges to the side of greater wedge thickness. This can cause difficulties in measuring the changes in height in certain cases.   It is particularly noticeable when using fringes of equal chromatic order.

9.8 REFLECTING FILMS

The choice of a reflecting film depends mainly on the reflectivity at the wavelength desired and the absorption. Other factors of importance are the mechanical strength and contouring properties.   Two types of metal films are used,

silver and aluminium.   In the present work silver has been
used since it has a higher reflectivity with minimal absorption
The film is produced by thermal evaporation at a pressure of
less than 5×10^{-5}m.m. Hg, in an Edwards evaporation unit.   For
a reflectivity of 0.9 the film thickness is 500 A.U.   It has
been verified by Bhide (1956) that a film of this thickness
has good contouring properties.   He experimented with the
sharp steps of the growth spirals on SiC crystals and found
that the step height was reproduced exactly up to a large · · .
thickness (6,000 A.U.) of the evaporated film.   The contouring
properties of multilayer dielectric films are not good near a
step but are adequate for a reference flat.   Since these films
are robust and of low absorption they were used extensively in
the work described, as the front reference flat.

9.9 HIGH-REFLECTING MULTILAYER FILMS

It has already been remarked that these can have a high
reflectivity with very low absorption.   The film consists of
layers of dielectric of alternately low and high refractive
indices (with respect to the substrate), each layer of optical
thickness $\lambda/4$.   The properties of these films have been dis-
cussed in detail by Heavens (1955).

The principle of multilayer films can be most readily
understood by consideration of a single layer.   If a layer of
optical thickness $\lambda/4$ is deposited on glass, the reflectivity
is increased if the refractive index of the film is greater
than that of the glass.   The light reflected at the

π

$O+\pi$

$\pi+2\pi$

$O+3\pi$

OPTICAL
THICKNESS

PHASE CHANGE ON
REFLECTION

$\lambda/4$ μ_1 π / O

$\lambda/4$ μ_2 $\mu_1 > \mu_2$

$\lambda/4$ μ_1 π / O $\mu_1 > \mu_3$

GLASS μ_3
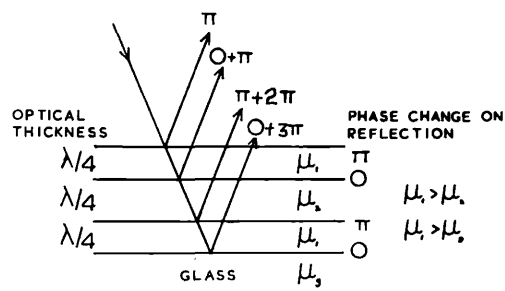
Fig. 9.3

dielectric-air surface suffers a phase change of π and is in phase with that reflected at the dielectric-glass surface which has traversed an additional optical path of $\lambda/2$, this being equivalent to a phase change of π. Thus the light reflected from both surfaces is in phase, giving rise to the higher reflectivity. If the film has a refractive index lower than the glass substrate, the light reflected at the upper and lower surfaces is out of phase, and an anti-reflection surface is formed.

The reflectivity of a single $\lambda/4$ layer is given by

$$R = \left[\frac{\mu_2 - \mu_1^2}{\mu_2 + \mu_1^2}\right]^2$$

where μ_1 is the refractive index of the film and μ_2 that of the substrate. If $\mu_1 = 2.38$ (zinc sulphide) and $\mu_2 = 1.5$ the value of R obtained is 31%. By using a number of films of alternately high and low refractive index each of optical thickness $\lambda/4$, high reflectivities can be obtained. For an odd number of layers the refractive index order on a glass substrate must be G (glass), H (high), L (low), H to ensure that the light reflected from each interface is in phase. This is shown diagramatically in fig. 9.3.

The films are deposited by thermal evaporation in a vacuum, the conditions being similar to those required for metal films. It is necessary however to control the thickness of each layer during the deposition process. A convenient and precise method is to measure the reflectivity with a photo-cell.

Another method of control is by the visual observation of the
colour change in the reflected light, Banning (1947).
Although not precise it is sufficiently accurate for many
purposes, and only reqires a lampand an observer. The per-
mitted tolerance in a layer thickness is quite high, Dufour and
Herpin (1954) quote a value of 10%.

The colours of ZnS and cryolite films as seen in reflec-
tion with white light at normal incidence are shown in Table. 1.

TABLE 1

Optical Thickness = 5461 A.U.	Colour	
	ZnS	Cryolite
$\lambda/4$	bluish white white greenish yellow	yellow magenta blue
$\lambda/2$	magenta blue	white yellow
$3\lambda/4$	greenish white yellow magenta	magenta blue greenish white

It is necessary to include a monitor plate with an adjustable
shutter so that each layer can be viewed separately. Satis-
factory results were obtained by this method, for 5 layer films,
which were used for the front surface of the interferometer in
the present work.

An advantage of films made of the above materials is that

they are resistant to scratching (important when a metal surface is being examined) and do not deteriorate on exposure to the atmosphere, thus the films can be used for long periods.

9.10 EXPERIMENTAL PROCEDURE

The glass flats, or specimens to be coated, are washed with detergent and water, dried and rubbed gently with cotton wool. Care had to be taken to avoid scratching the soft Perspex specimens. They were then placed in the evaporating plant, a filament-target distance of 25 cms. ensuring even coating. At a pressure of 0.2m.m. Hg, a high tension discharge was passed for a short time to clean by ionic bombardment. The pressure was then reduced to about 5×10^{-5}m.m. Hg, and the material evaporated. The thickness of the metal films was controlled by evaporating for a known time under standard conditions. Alternatively, a fairly good estimate of the thickness can be obtained, with practise, by viewing the filament through the film while the silver is being deposited.

9.11 FIZEAU FRINGES

The surface to be studied and the flat are placed in contact in a jig with three spring loaded adjusting screws, so that the wedge angle can be varied as required. Parallel monochromatic light must be incident on the interferometer and this is obtained with the optical set-up shown in fig. 9.4. The image of the light source is formed at the back focal

plane of the objective.   Thus light emerges from the objective
as a parallel beam and falls normally on the interferometer.
The objective is focussed on the surface of the wedge and thus
the fringes are seen in the image plane of the microscope.
The Fizeau fringes are treated as contour lines and a diametral
section of the surface may be plotted along a line parallel to
the undistorted fringes i.e. where the wedge thickness is con-
stant.   This method gives the shape of the surface distortion.
The depth of a depression can be determined by counting the
number of fringes contained in it.

9.12 FRINGES OF EQUAL CHROMATIC ORDER

These fringes, obtained with white light, were described
by Tolansky (1945).

The formula for these fringes is

$$2\mu t \, \text{Cos} \, \phi = n\lambda, \qquad \text{if} \, \mu = 1 \text{ and } \phi = 0$$

we have $\qquad 2t = n\lambda$

If λ is variable, fringes of equal t/λ can be produced if the
light is dispersed in a spectrograph.

The optical arrangement is shown in fig. 9.5.   A is a
white light source which illuminates the aperture C by means
of the condenser lens B.   The lens D produces a parallel beam
which is incident on the interferometer E.   The lens F
projects an image of the localised fringes on to the slit G of
the spectrograph.   The slit selects a line section of the
interference film and should be parallel to the edge of the
wedge.   Then chromatic fringes are produced,in the eyepiece
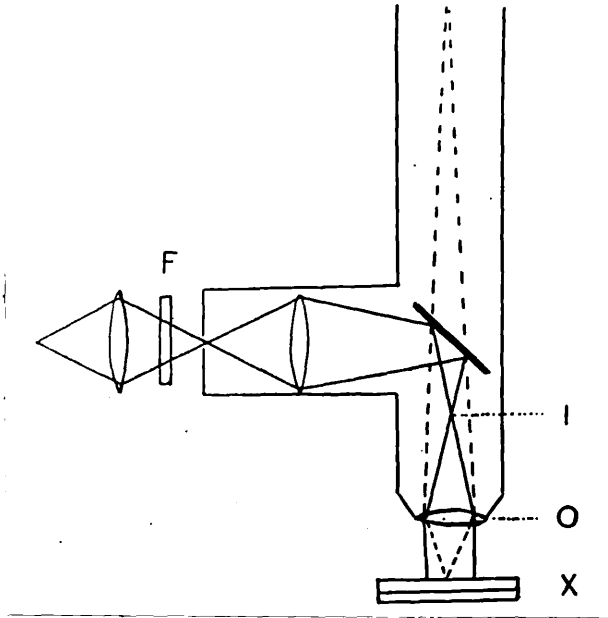
FIG. 9.4
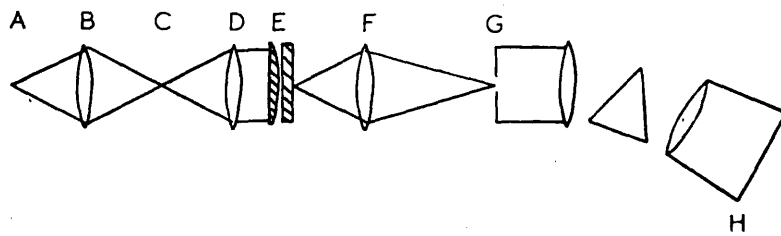
FIG. 9.5
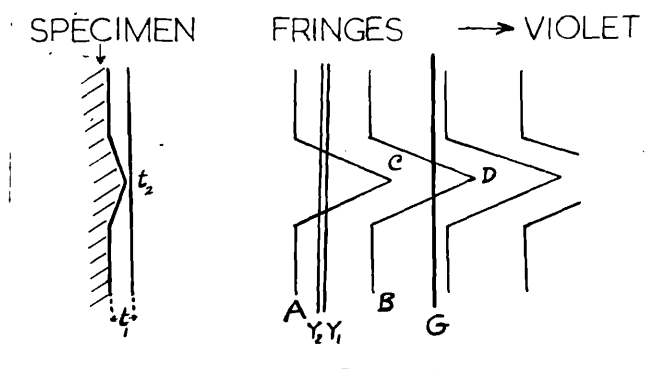
FIG. 9.6

of the spectrograph.   Since the fringes are lines of constant
t/λ any slight variation in thickness Δt will cause a change in
the wavelength $\Delta \lambda$ at that point given by $\Delta t = n \Delta \lambda$

Consider the section of the surface under study which is
imaged on the slit of the spectroscope.   Suppose the inter-
ferometer thickness changes in the manner shown diagramatically
in fig. 9.6.   The equal chromatic order fringes will be
parallel to the spectroscope slit at the top of the field
where the thickness is constant, deviate to the violet as t
decreases and then return to their original positions.   Thus
the fringes are a profile of the surface of the specimen, along
the line imaged on the slit.

The dispersion depends on the separation of the surfaces
and not on the wedge angle.

9.13 METHOD OF MEASUREMENT

Suppose the height of the hill shown in fig. 9.6 is to be
measured.   If n is the order of the fringe A, then the order
of the next fringe B is (n+1).

Then the interferometer gap t_1 is given by

$$2t_1 = n\lambda_A = (n+1)\lambda_B$$

Thus
$$n = \frac{\lambda B}{\lambda_A - \lambda_B}$$

Similarly
$$2t_2 = n\lambda_C = (n+1)\lambda_D$$

Hence
$$2(t_1 - t_2) = 2\Delta t = n(\lambda_A - \lambda_C)$$

This gives
$$\Delta t = \frac{1}{2} \frac{\lambda B}{\lambda_A - \lambda_B} (\lambda_A - \lambda_C)$$

where $\triangle t$ is the height of the hill shown.

The two fringes A and B selected for measurement should preferably be near the Hg green and yellow lines.

The distance between the yellow line Y_1 and the green line G give the wavelength scale, so that the displacements at A and C etc. can be read off as wavelength changes from the dispersion curve of the spectrograph. Alternatively, a Hartmann formula can be used.

These fringes give a very large vertical magnification, the limit being set by the surface finish and uniformity of the distorted region. A disadvantage compared with Fizeau fringes is that an overall picture of the distorted region is not obtained, the measurement being confined to a line section which can lead to considerable error in interpretation if the distorted region is irregular.

CHAPTER 10

FALLING BALL AND DROP EXPERIMENTS

10.1 DROPPING STEEL BALLS

This was in the nature of a preliminary investigation, conducted before the gun was built, to get an idea of the general nature of the damage caused by impact on "Perspex". A range of ball sizes and heights was used, the heights being those that could be simply obtained, such as the College lift shaft. The ball sizes ranged from 5/16 in. to 1.7/8 in. diameter, and the height from 1 ft. to 43 ft. The specimens were usually cut about 2 ins. square and the thicknesses used were 1/8, 1/4 and ½ in. They were clamped to a steel or wood block, and with some of the specimens a layer of grease was applied which gave better contact as shown by the increase in rebound height when using a thin specimen. Some experiments were also made with the specimen gripped at the edge only. The general effect of changing from a freely supported specimen to a clamped one was to reduce breaking due to bending stresses and to favour fractures at the front surface by Hertzian forces. With thick specimens and small balls however, the type of support had little effect on the nature of the damage. This is as might be expected and is as given by Zener's inelasticity parameter which shows that the Hertz elastic equations hold in the case of specimens thick compared with the ball size. As a general conclusion it may be said that, at low velocities with large balls radial
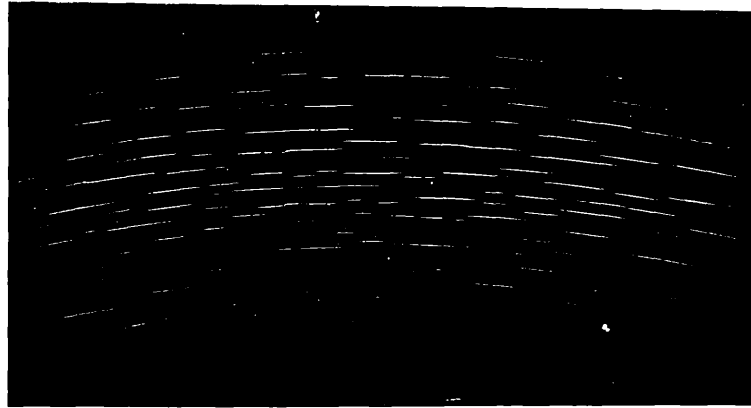
FIG. 10.1   X50
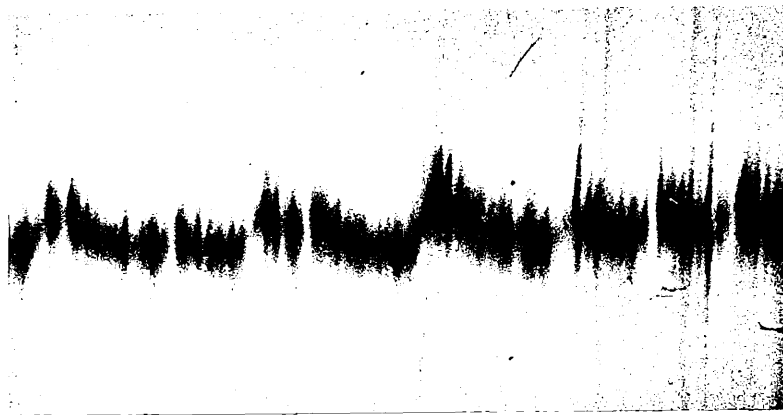
FIG. 10.2   X300
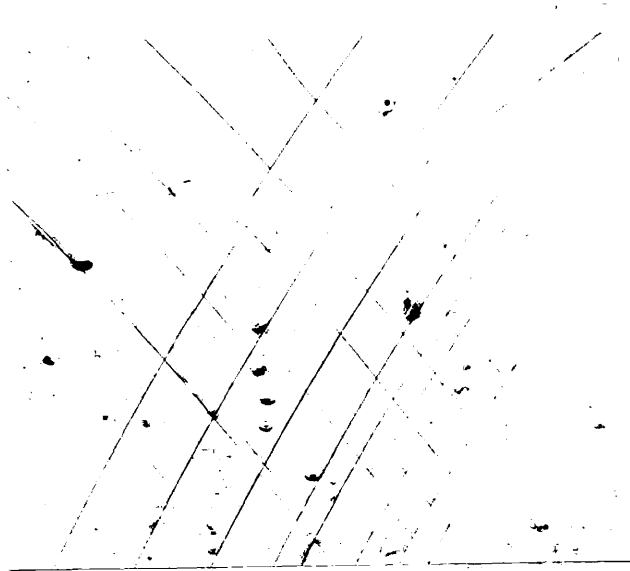
FIG. 10.3   X460

cracking occurred from a point directly opposite the impact region, often with a superimposed ring or cone shaped crack. At higher velocities, with smaller balls the damage consisted of an annular region of fine cracking or crazing. No plastic deformation of the material was observed.

10.2 RESULTS

Fig.10.1 shows the crazed region taken with oblique incidence so that the edges of the cracks show up. A part of the annular region of short curved fine cracks can be seen. The surface pile-up at a crack was measured using equal chromatic order fringes, fig. 10.2. The height of the pile-up is of the order of 150-200 A.U. A region where the crazing cracks crossed, because of overlapping impacts, was examined using Transmission Phase Contrast illumination. It can be seen in fig. 10.3 that the cracks appear to cross one another without any deviation or interaction.

10.3 DEPTH OF CRACKS

The depth of the cracks is of considerable importance, as by Griffith's theory the strength of the material depends upon it.

Griffith (1921) considered the two dimensional case, where the crack is regarded as an ellipse of small minor axis, i.e. a plate with an elliptic cavity going right through it. He found that the rupture stress is proportional to $C^{-\frac{1}{2}}$ where 2C is the crack length for internal cracks, or C the depth of

surface cracks.   This theory has been extended to the three

dimensional case by Sack (1946) with essentially the same .

result.

The depths of the crazing cracks produced by the impact

of a 7/16 in. steel ball from a height of 36 ft. have been

measured by the technique described previously.   Fig. 8.3

shows the cracks.   The maximum depth of about 0.05 m.m.

occurs at the centre of the cracked region.   Bartoe (1943)

has reported a marked dependence of Charpy notched impact

strength on the depth of surface scratches in "Perspex".

10.4 FALLING MERCURY DROPS

Since in either of the theories of liquid drop impact the

pressure developed is proportional to the density of the liquid

(apart from a multiplying factor which depends on the velocity)

damage might occur at a much lower velocity with mercury drops

than with raindrops.

A dropper similar to that used by Worthington 1877 was

used, and mercury drops were allowed to fall through a height

of up to 43 ft., the drop size being about 4-5 m.m.   Neglect-

ing air resistance, the terminal velocity v in ft./sec.

reached from a height h ft. is given by

$$v = 8h^{\frac{1}{2}}$$

thus when h = 43 ft., v = 53 ft./sec.   Since the specific

gravity of mercury is 13.6, and the multiplying factor can be

taken as 0.7 (Engel 1955), this is equivalent to a raindrop

moving at 500 ft./sec., which might be fast enough for damage to occur. No impact mark was observed however in these experiments. It is possible that, due to air resistance, a velocity of 50 ft./sec. would not be reached, but since the terminal velocity of 5 m.m. waterdrops is 30 ft./sec., Davies (1939), mercury with its greater density would be expected to gain a considerably higher velocity.

CHAPTER 11

SOLID SPHERE IMPACT

11.1 IMPACTS ON PERSPEX

Impacts have been made with both steel and glass spheres on specimens of polymethyl methacrylate or Perspex. This substance was chosen partly because of its direct interest as a constructional material, and because it would be expected to behave essentially as an elastic solid when subjected to high speed impact. In addition the polymer is readily available in sheet form with an excellent surface finish.

Two types of the material are made, unplasticised and plasticised, the latter having a lower softening point. All experiments were performed on unplasticised material. The specimens were cut from ½ in. thick "Commercial" sheet to a size 1½ ins. square using a circular saw.

11.2 STEEL BALLS

Steel balls of 7/32 in. and 11/64 in. diameter were shot at velocities ranging from 100-700 ft./sec. A typical damage site is shown in fig. 11.1. At a velocity of about 100 ft/sec. damage occurs and consists of an annular region of short, curved, fine cracks or crazing. As the velocity is increased the diameter and area of the region grow and the outer edge terminates in a complete circular crack from which radial cracks may emerge. These cracks can penetrate the material
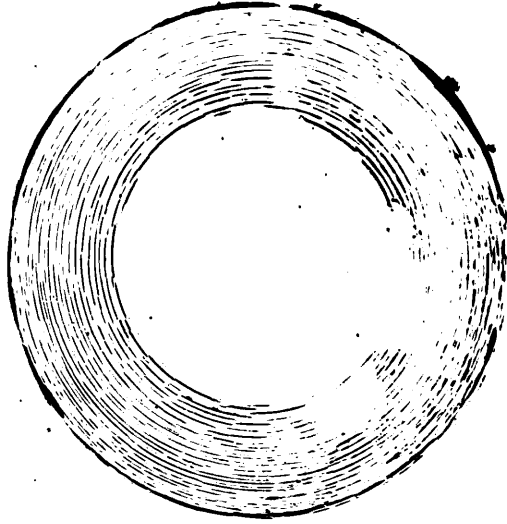
FIG. 11.1   300 FT./SEC.   X 27
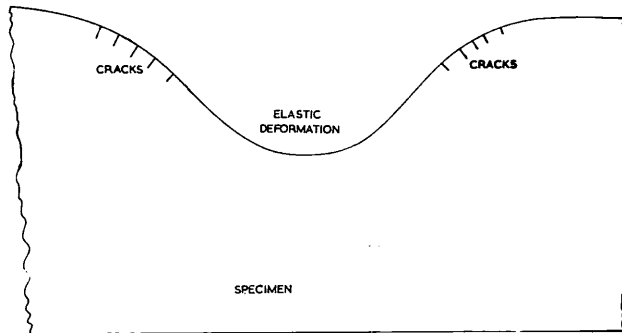
FIG. 11.2

obliquely until they meet thus removing a surface layer. A slight spherical depression at the centre of the impact site was observed at the higher velocities.

The cracked region was scanned using the light profile. Major surface displacements occur at relatively few of the cracks, steps of the order of 1μ were observed. The central region is displaced below the general surface level, i.e. all the displacements at the cracks were downwards, going from the outside edge to the centre. A similar effect was observed by Howes (1955) in ring cracks on glass. It is probably caused by the cracks closing up on removal of the stress and preventing complete recovery. The closing up effect also produces a piled-up region on each side of the cracks as shown in Chapter 10.

The impact process can thus be described as follows: When the ball strikes the surface it deforms elastically to a shape similar to that shown in fig. 11.2. There will be radial tensile stresses down the sides of the depression. These will be a maximum at the edge and decrease towards the bottom where in addition the material is under compression which reduces the tendency to fracture. Thus cracks will be formed in an annular region. The diameter of the circle of cracking should correspond with the circle of contact between the ball and the surface. This was checked by firing steel balls ground with 800 Carborundum. These mark the surface and enable the area of contact to be determined. In all cases

the outer limit of the roughened area coincided with the circle of cracking.

The outer diameter of the cracked region was measured in two directions at each velocity and results are shown in Table 2. The mean value was plotted against the velocity on a log-log scale, fig. 11.3. The experimental points lie on a straight line which indicates a law of the form,

$$d = Av^n$$

This law appears to hold over the velocity range investigated where d ranges up to ¾ diameter of the ball.

A similar result for static indentations made on a variety of polymers is reported by Pascoe and Tabor (1956).

Since the impact is essentially elastic the experimental results can be compared with the Hertz theory.

The relation between the radius of the circle of contact and the velocity is

$$a = \left\{1.25\pi\rho_1\left(\frac{1-\sigma_1^2}{E_1} + \frac{1-\sigma_2^2}{E_2}\right)\right\}^{1/5} Rv^{2/5}$$

This equation is of the same form as that given above, so that the value of A should depend on the nature of the ball and the impact surface and be directly proportional to the radius of the ball. Thus for true elastic deformation n = 0.4.

The value of n obtained experimentally is 0.42, and the diameter of the circle of contact appears to be proportional to the ball radius. Thus it appears that the Hertz theory holds fairly well for impacts in this velocity range.
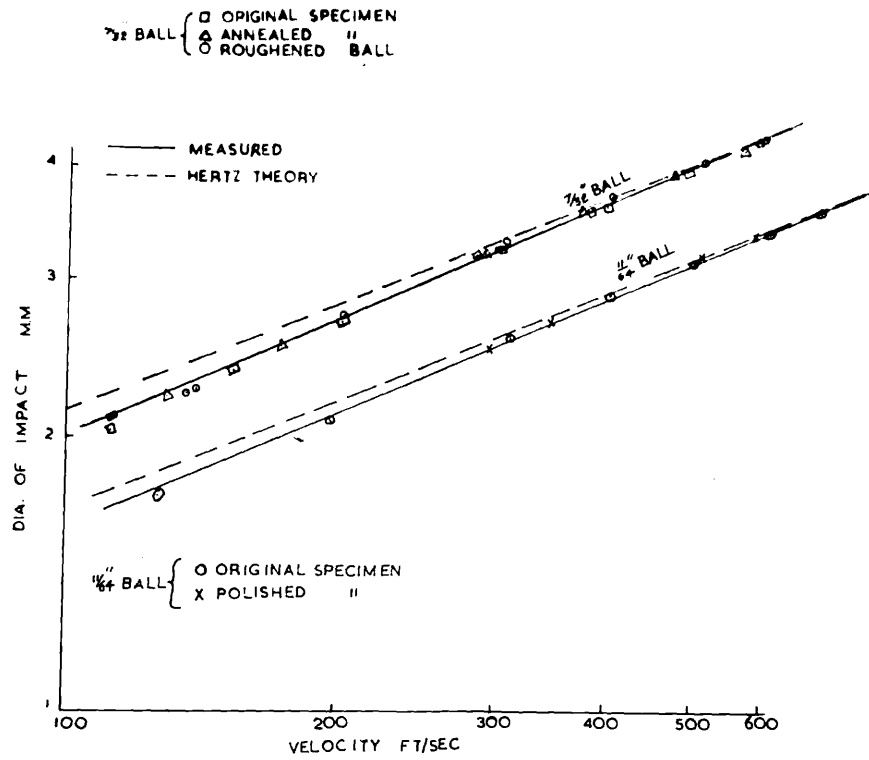
FIG. 11. 3
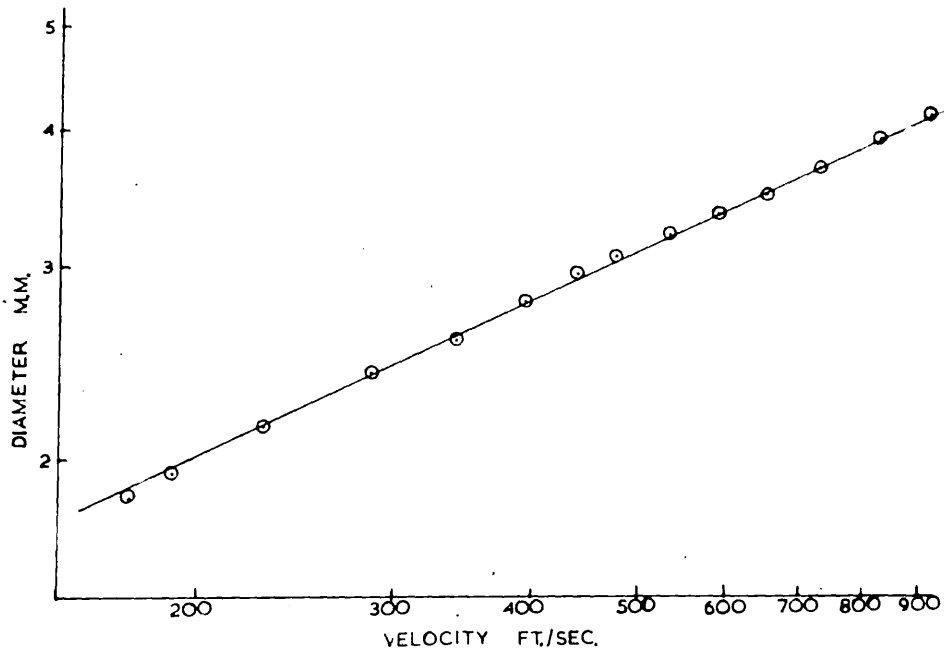
FIG. 11. 4

TABLE 2

7/32" STEEL BALL						11/34" STEEL BALL			
NORMAL SPECIMEN		ANNEALED SPECIMEN		ROUGHENED BALL		NORMAL SPECIMEN		POLISHED SPECIMEN	
VEL.	MEAN DIA.	VEL.	MEAN DIA.	VEL.	MEAN DIA.	VEL.	MEAN DIA.	VEL.	MEAN DIA.
113	2.04								
		129	2.22	136	2.23	127	1.71	298	2.5
114	2.10	150	2.38	139	2.26	197	2.12	349	3.0
157	2.38	173	2.53	153	2.39	312	2.60	518	3.24
202	2.71	293	3.23	204	2.74	405	2.91	597	3.4
287	3.22	378	3.62	310	3.33	507	3.19		
304	3.25	481	4.00	408	3.76	620	3.43		
306	3.27	578	4.24	521	4.12	708	3.63		
386	3.60	607	4.35	612	4.38				
403	3.65								
498	4.04								
600	4.36								

where vel. is measured in ft/sec
and dia. is measured in m.m.

Values of the diameter of contact were calculated, taking

E_1 = 2 x 10^{12} dynes/sq.cm., for steel

E_2 = 3 x 10^{10} dynes/sq.cm., (Static Value) for Perspex

and plotted as shown. The modulus E_2 for perspex will

probably be larger than that assumed as it will depend on the

rate of deformation. This would effectively shift the graph

downwards. The theory is derived assuming small deformations,

and thus is not strictly applicable for the higher velocities.

The agreement is good enough however to show that the forces

controlling the damage at the impact site are Hertzian in

nature.

Impacts were also made on specimens which had been

previously annealed, Russell (1949), and on specimens polished

with I.C.I. Perspex polish, Table 2. These treatments did

not appear to have any noticeable effect on the magnitude of

the damage, and the results are plotted for comparison in

fig. 11.3. There was a marked tendency however for the

crazing cracks on the polished specimens to be straight lines

rather than arcs of circles.

The tensile stress at the edge of the circle of contact,

corresponding to the minimum velocity of about 100 ft./sec.

required to cause crazing cracks was also calculated from the

Hertz equation. These give a value of about 8 x 10^8 dynes/sq.

cm. or 12,000 lbs./sq.in. The corresponding value for a

static tensile test on untreated material is about 50% of the

tensile strength of 10,000 lbs./sq.in.

11.3 GLASS SPHERES

To extend the observations to include another type of
solid impactor, and to increase the velocity range, glass
spheres were used. The density of glass is about 1/3 that of
steel, thus enabling a higher velocity to be attained. The
spheres were unharmed after impact on Perspex. The spheres
were obtained in the form of ballotini, but these were not
truly spherical and gave very erratic results. They were
ground with 800 Carborundum between two contra-rotating
eccentric steel laps until spherical to within 0.0005 in., and
then polished by shaking for some time in a paste of alumina
and water. The finish was not good but was of sufficient
quality to enable the surface damage to be seen under the
microscope. The damage site was similar to that observed in
steel ball impact, the crazing cracks being circular. The
roughened region extended up to the outer circular crack,
showing again that this coincided with the circle of contact.
This roughening did not cover the whole area, but a circular
patch in the centre was smooth. The size of this region
decreased with increasing velocity.

Impacts were made in the velocity range 100-900 ft./sec.,
results are given in Table 3. The diameters of the circular
cracks were plotted against the velocity fig. 11.4. It can
be seen that the graph is fairly linear over the whole range.
Thus as before a relation of the type $d = kv^n$ is valid.
For the graph $n = 0.46$.

TABLE 3

0.218 in. Diameter Ground and Polished Glass Balls.

Vel. ft./sec.	173	190	229	285	341	393	441
Mean Dia. m.m.	1.84	1.93	2.14	2.40	2.57	2.79	2.96
Vel. ft./sec.	478	553	594	657	734	838	932
Mean Dia. m.m.	3.06	3.21	3.35	3.50	3.70	3.93	4.14

TABLE 4

Vel. ft./sec.	Dia. m.m.	Depth m.m.	Vol. $\times 10^{-3}$ c.c.	$(Vel.)^2$	Log. Vel.	Log. Dia.
586	3.25	0.626	2.73	34340	2.768	0.512
623	3.33	0.668	3.07	38813	2.795	0.522
678	3.46	0.669	3.30	45968	2.831	0.539
752	3.69	0.796	4.52	56550	2.876	0.567
785	3.77	0.884	5.26	61623	2.895	0.576
855	3.89	0.937	6.01	73103	2.932	0.590
892	3.99	1.004	6.81	79566	2.950	0.601

11.4 DISCUSSION

Over the whole velocity range for both steel and glass impacts a relation of the type d = kv^n fits very well.

Steel ball impact is essentially elastic and can be described by the Hertz equations. The agreement is not so good for the glass ball impact, the diameter increasing more rapidly with the velocity.

These results suggest that the Hertz theory can be applied to impacts under these conditions, and that the forces controlling the behaviour of a surface under impact by a liquid drop would be of this nature.

11.5 STEEL BALL IMPACT ON METALS

11/64 in. steel ball bearings were fired at a Duralumin block size 1¼ ins. square and ½ in. thick, at velocities ranging from 600-900 ft./sec. The surface of the block was polished with alumina on a rotating Selvyt lap. On inspection the craters appeared to be hemispherical depressions, the impacted region having the mirror finish of the impacting ball bearing. Pronounced ridging occurred round each indentation, the edge of the ridge appearing somewhat jagged when viewed under the microscope. A marked roughening and distortion of the surface was observed in a region round the dent extending to about twice its diameter. The diameter of the indentation was measured for each velocity. The depth of the depression was determined by alternately focussing on the bottom of the

indentation and on the surface of the specimen, and reading
off the depth from the fine focussing screw of the V.P.M.,
which was calibrated in microns.   The calibration was checked
using a 0.050 in. slip gauge rung on to another gauge.
Assuming that the indentations are spherical the volume can be
calculated from the known depth and diameter.   The results are
shown in Table 4.   The measurement of the diameter of an
indentation is complicated by the contour near the edge.   It
has been suggested that since the ball is in contact with the
metal forming the ridge, this "piled-up" portion supports its
share of the load and should be considered as the true
diameter of the indentation, (O'Neill 1934, Turbadar 1957).
Some experiments by Bergsmann (1954) indicated that the piled-
up region did not support any of the load and that the true
size of the indentation is that diameter corresponding to the
original surface level.   There is some evidence however that
these experiments were not conclusive (Tabor 1957, private
communication).   The indentations measured here however, are
so deep that the difference in the two diameters must be small.
The edge is easy to locate and this diameter was measured.
The hardness of the Duralumin specimen used was determined
using Brinell type hardness tester at various loads.   A plot
of load against diameter on a log-log scale gave the Meyer
index of the specimen = 2.1.   This showed that the material
was almost fully workhardened, thus effects due to further
workhardening in the impact test would be minimised.   The

B.H.N. = 115, at the recommended load of 10 Kg. The diameter of the indentation is plotted against the velocity in fig. 11.5 on a log-log scale. The points lie on a straight line, of slope 0.48.

Thus $$d = kv^m$$ where m = 0.48.

Kokado (1927) deduced a relation between the Meyer index n and the exponent m of the above curve. The relation is

$$m = \frac{2}{n+2}$$

Thus when n = 3, for a perfectly elastic impact m = 0.4 as given by the Hertz theory. When n = 2, as in the case of an ideal plastic material, we have m = 0.5. Putting m = 0.48, we have n = 2.15, which is in agreement with the static value of the Meyer index obtained above. This second relation can be derived from the fundamental concept that the kinetic energy of the indentor is proportional to the volume of the indentation. Early workers (Vincent 1900) have confirmed this idea, although the precision of their experiments was not high. More recently Valkenburg, Clay and Huth (1956) have reported it to be valid in a velocity range up to 5,000 metres/sec. They do not discuss however either their method of measuring the volume or what volume was measured. The volume displaced due to the kinetic energy of impact is considered to be that below the original surface level, as it would not be reasonable to include that enclosed by the sharp edge which is formed by flow of material during the impact. Now the constant in the above equation is equal to the average dynamic pressure p'
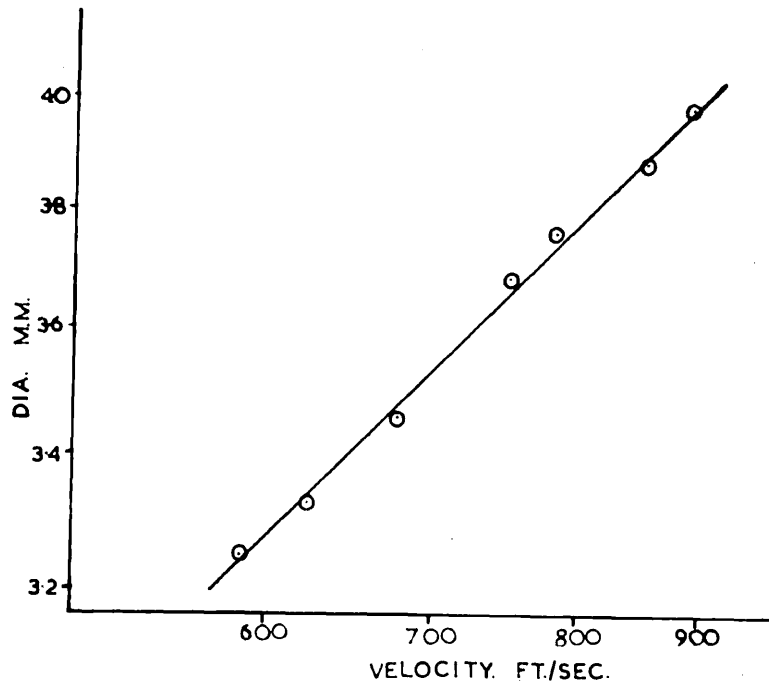
FIG. 11. 5
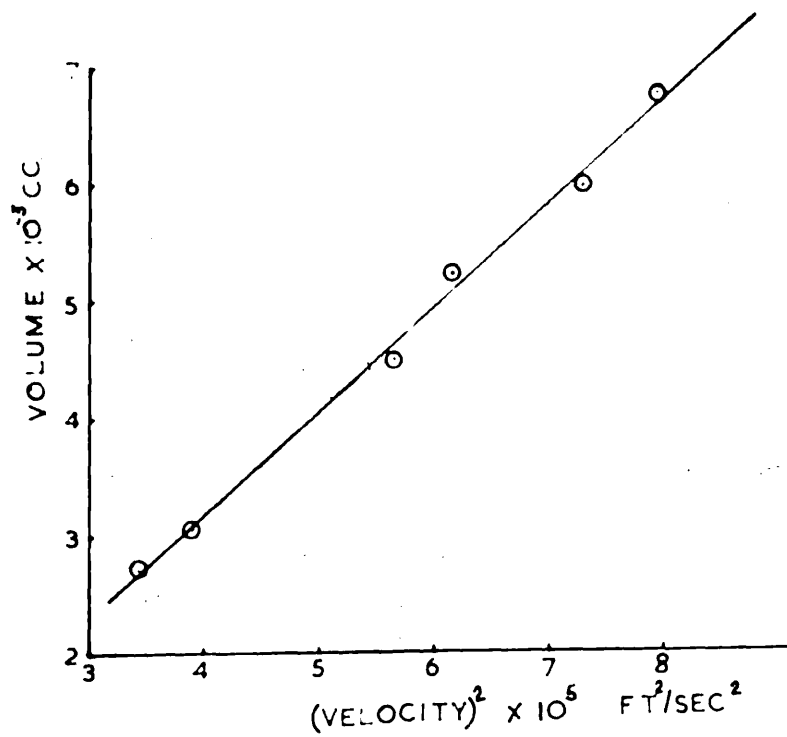
FIG 11. 6

exerted during impact. The volumes of the indentations were calculated from the formula

$$V = \frac{1}{6}\pi h(h^2 + \tfrac{3}{4}d^2)$$

where h = depth of indentation and d = diameter of indentation, and plotted against the kinetic energy of the impactor, giving a linear relationship as shown in fig. 11.6.

The discussion above neglects the rebound energy of the indentor in comparison with the initial energy. This is a reasonable assumption considering the large amount of plastic deformation which occurs at the high velocities used. Any variation in the value of p' is also neglected. This would tend to increase with velocity due to workhardening and the large amount of energy needed in the kinetic displacement of the metal around the indentation.

There is some evidence (Campbell and Duby 1956), that the workhardening due to a dynamic stress, is much less than that occurring under static conditions.

11.6 INITIAL YIELD STRESS

From a measurement of the minimum height of fall required to produce a perceptible indentation, using a steel sphere as a pendulum (Davies 1949), a value for the initial dynamic yield stress can be determined. The Hertz equations are used for calculating the mean normal pressure over the indentation, which by either the Tresca-Mohr or Huber-Mises criterion of yielding equals 1.1Y where Y is the yield stress referred to.

The equation is (Chapter 5),

$$p = \frac{4}{3\pi}(1.25\pi\rho)^{1/5}\left(\frac{E_1 E_2}{E_2(1-\sigma_1^{2})+E_1(1-\sigma_2^{2})}\right)^{4/5} v^{2/5}$$

where $E_1 = 2\times10^{12}$ dynes/sq.cm., $E_2 = 6.9\times10^{11}$ dynes/sq.cm., $\sigma_1 = 0.286$, $\sigma_2 = 0.34$, $\rho = 7.8$. The height h required was from 0.05-0.1 cm. giving v = 10-14 ft./sec. Thus we have

$$p = 5.6-6.4 \times 10^9 \text{ dynes/sq.cm.}$$

Hence the dynamic yield stress = $5.1-5.8 \times 10^9$ dynes/sq.cm.

The value of the static yield stress obtained from the Brinell hardness determinations mentioned previously is $4.0-4.5 \times 10^9$ dynes/sq.cm. This increase in the dynamic yield over the static yield corresponds with that obtained by Campbell (1953) for uniaxial compression of an Al-Mg alloy. Taylor and Whiffen 1948 obtained a ratio of 1.4 with Duralumin of B.H.N. = 118, in the velocity range 1,000-2,000 ft./sec. Even if no workhardening occurs, and p' is not velocity sensitive, its value will depend on the size of the indentation, corresponding to the transition from the onset of deformation to full plasticity. From the calculations given by Ishlinsky and static hardness experiments, we would expect the mean pressure over a fully plastic indentation to be equal to about 2.8/1.1 = 2.5 times the pressure required to initiate plastic deformation. The value of p' is calculated from the slope of the line in fig. 11.6, p' = 1.57×10^{10} dynes/sq.cm. The value of the ratio . of the initial dynamic yield pressure to the yield pressure for full plasticity is thus:

$$\frac{15.7 \times 10^{10}}{5.6\text{-}6.4 \times 10^9} = 2.6$$

which is in agreement with the above analysis.

11.7 CONCLUSIONS

A relation of the type $d = kv^n$ appears to fit over the velocity range considered, and the volume of the indentation is proportional to the energy of impact. The relation between the pressure required to produce a fully plastic indentation and that for the initial yielding is of a similar magnitude to that required in the static case.

CHAPTER 12

POLYTHENE PELLET IMPACT

12.1 INTRODUCTION

It was thought that the study of the impact of a deform-
able solid, which would be a transition stage between solid-
solid and liquid-solid impact might yield useful information.
Polythene was chosen because it deforms readily and is of very
low density enabling high velocities (up to 1,250 ft./sec.)
to be acheived.   The possibility also arises that since it is
simpler to fire a polythene sphere at a specimen, than to
project the specimen at a water drop, this might provide a
similated dropimpact test of sufficient accuracy for the test-
ing of materials for rain-erosion properties.

12.2 DESCRIPTION OF PELLETS

The pellets were injection moulded from I.C.I. Grade 20
polythene.   One half of the pellet was a hemisphere, but there
was a moulding ridge around the equator and a flat on the other
half.   Some pellets were fired in the "as-received" condition,
but the results were not reliable, since they hit the specimen
at differing orientations, which effectively varied their
radius of curvature.   For satisfactory results it was essen-
tial that the hemispherical part of the pellet hit the specimen
normally.   This was acheived by moulding the pellets into
short cylinders, i.e. reducing the diameter of the equatorial
moulding ridge, and loading with the hemispherical region

towards the target.   By placing this fairly close to the end
of the gun barrel, the pellets hit normally.   The safety tube
had to be shortened considerably and the end of the barrel
brought close to the first photo-cell.   In addition, a slight
constriction was necessary at the end of the safety tube, to
ensure that the pellets did not yaw.   The orientation of the
pellet on striking, could be determined by examining the
deformed pellet.   In general the pellets made contact, such as
to present a constant radius of curvature to the impacted sur-
face.   The mean radius of curvature of the pellets = 2.50m.m.
The diameter corresponded to the smallest barrel size of
11/64 in.   Average mass of pellet = 52.0 m.gms.

12.3 IMPACTS ON PERSPEX

Pellets were fired at specimens of unplasticised Perspex
1½ ins. square and ½ in. thick, in the velocity range 700-
1,250 ft./sec.   The specimens were examined under the
microscope at low magnification, to see the nature of the
polythene wash left on the surface.   Then this smeared
material was gently washed off, and a layer of silver evapor-
ated on to the surface.   The enhanced reflectivity enabled
the surface details to be seen more clearly.   Fizeau inter-
ferograms were taken of each impact site, enabling the size and
depth of the indentation to be measured, and the distribution
of cracks seen.   All measurements of the diameter etc. were
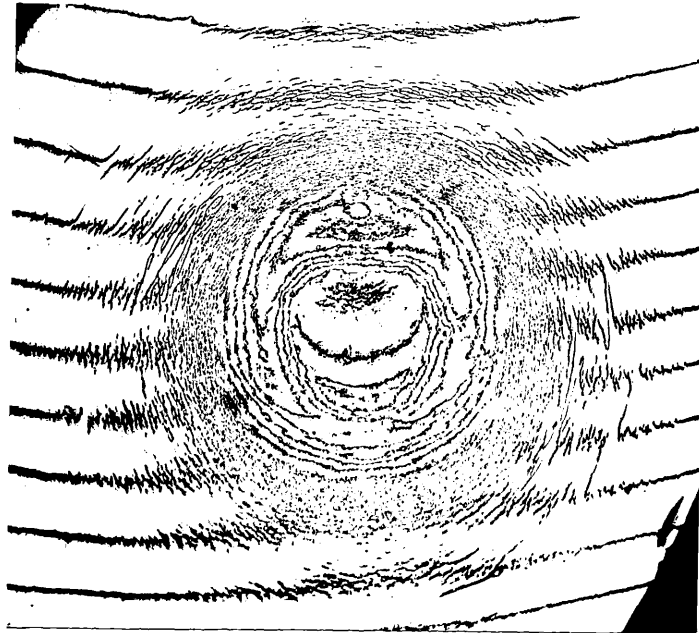made from the Fizeau photographs, as on these the edge is more
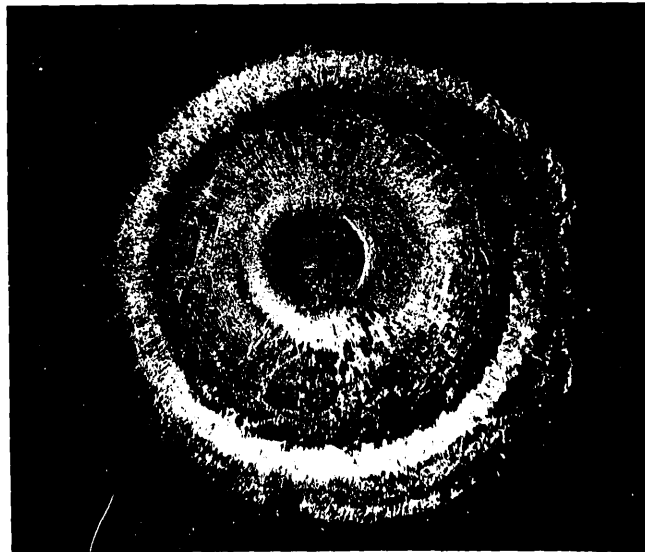
FIG. 12. 1   980 FT./SEC.   X 19

FIG. 12. 2   1250 FT./SEC.   X 9

easily determined than from a normal picture. The inter-
ferogram obtained from a typical impact site is shown in fig.
12.1. This can be compared with fig. 12.2 taken with oblique
illumination with the polythene wash on the surface.
Similarity between this damage site and that due to impact on
a water-drop is evident q.v. The damaged area consists of a
central region which is almost flat, surrounded by an annular
depression, (up to 3μ deep) which is enclosed by a region of
short circular cracks. These are similar to those occurring
in steel ball impact, but are shorter and less regular, there
being no well defined circular crack at the outer edge of the
region. The pellet deformed considerably at the higher   .
velocities, the impact surface becoming very concave. Poly-
thene was smeared over the surface of impact as a radial wash,
with an outer ring, as some reverse flow took place owing to
recovery of the pellet. The measured diameter of the pellet
after impact was in general about 80% of that of the maximum
diameter of the wash, and corresponded very closely to the
inner diameter of this ring. In a few cases a thin film of
material extended outside of this area. There was no marked
tendency for material to be removed from the outer edge of the
cracks by any flow of the pellet across them. (This effect is
noticeable in water-drop and lead shot impacts). It did how-
ever occur in some cases where rather longer straight cracks
were formed.
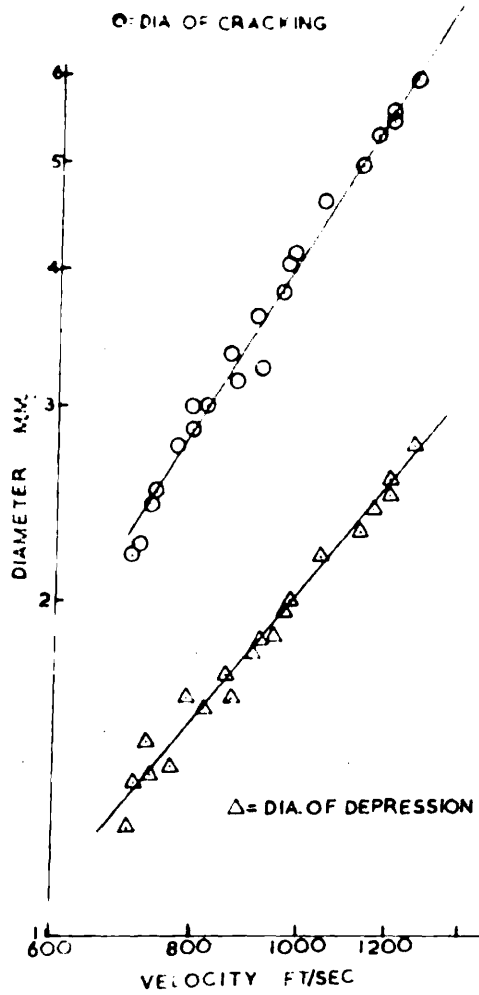
It is assumed that the cracks are formed as a result of

FIG. 12.3

the tensile stresses set up in the surface due to the spherical depression produced by the impacting pellet. Although the outer limit of the cracked region was not precise as in the steel ball impact, it was considered that the limit of the cracks would correspond to the region of overall deformation of the material. This diameter would thus approximately correspond to the diameter of the circle of contact in a solid ball impact, and also to the region on the surface weakened by the presence of cracks. The diameter was measured at each velocity of impact, Table 5. The results were plotted on a log-log scale, fig. 12.3. A straight line was drawn through the points, giving a law of the form $d = kv^n$ where $n = 1.63$ and $k = 4.18 \times 10^{-4}$ when d is in m.m. and v in ft./sec. A smooth curve could also have been drawn, but the accuracy of the results is not sufficient to really distinguish between the two. The rate at which this diameter of cracking increases with the impact velocity is thus much greater than that for steel ball impact.

The outer diameter of the annular depression was also measured and plotted against v giving $d_2 = k_2 v^{1.23}$ where $k_2 = 5.47 \times 10^{-5}$, fig. 12.3. The value of this depression was also determined. The Fizeau fringes are treated as con- tour lines of the surface. A line is drawn across the centre of the impact zone and a section of the surface plotted. The difference in level between adjoint fringes is 0.273 , the original surface level being determined from the undisturbed

TABLE 5

| VEL FT./SEC.	DIA. OF CRACKING M.M.	DIA. OF DEPRESSION M.M.	VOL. OF DEPRESSION x 10^{-7} c.c.
700	2.19	1.24	0.81
708	2.23	1.37	0.99
726	2.44	1.49	0.94
733	2.51	1.39	1.25
765	2.76	1.42	1.96
789	2.84	1.63	2.28
789	3.00	1.63	2.46
816	3.00	1.60	2.27
858	3.35	1.72	5.20
867	3.16	1.63	3.22
904	3.62	1.79	8.30
918	3.26	1.84	10.20
955	3.81	1.86	7.47
962	4.07	1.96	16.2
977	4.16	2.00	19.0
1040	4.62	2.19	27.1
1126	5.00	2.31	35.8
1160	5.35	2.42	40.9
1200	5.50	2.50	65.8
1200	5.62	2.58	67.3
1263	6.00	2.77	95.4

PELLET

1 μ

1 M.M.
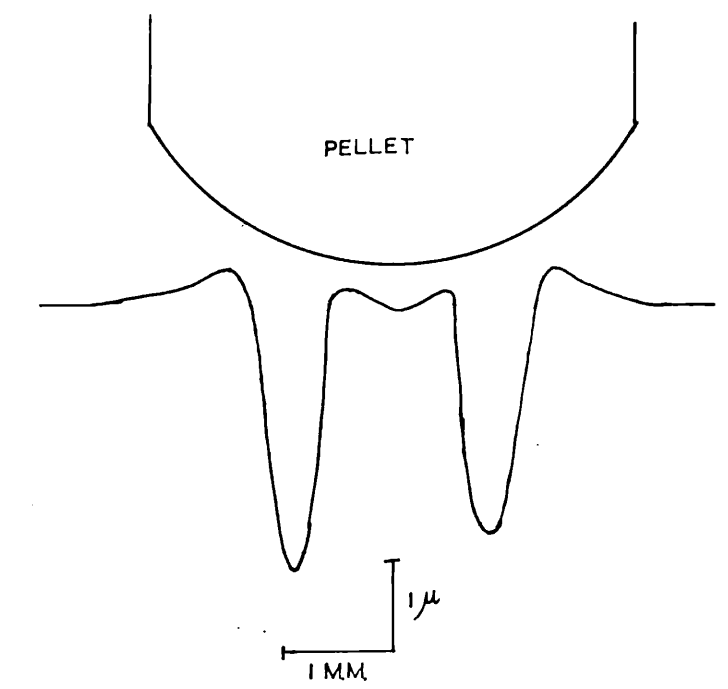
FIG 12.4

fringes outside the disturbed region.   A section is plotted
in fig. 12.4, with a section of the impacting pellet for com-
parison.   The horizontal and vertical magnification are shown.
To a first approximation the depression can be considered to
be of trapezoidal shape, where the bottom is ¼ width of the top.
The volume can then be easily calculated by measuring the inner
and outer diameters and the depth, Table 5.   The volumes are
plotted against the velocity in fig. 12.5.   A very rapid rate
of increase occurs, the law being

$$Vol. = Kv^{8.2}$$

12.4 STUDY OF THE CRACKS

The other features of interest on the impact site are the
depth of and surface distortion and displacement produced by
the cracks.   That considerable surface displacement does occur
is evident from the interferograms, but quantitative inter-
pretation is difficult on account of the diffraction effects at
the edge.   In the impacts at the highest velocities, above
1,000 ft./sec., an appreciable portion of the cracked region is
so broken up and disturbed that it is extremely difficult to
follow an individual fringe.   Here near the edge of the
depression many cracks occur with some overlapping.   Some sur-
face roughening due to the wash also occurs in this region.
Outside of this, the cracks become more widely spaced and
individual displacements can be seen, these being up to ½ a
fringe i.e. 0.1μ, gradually decreasing to about 0.02μ at the
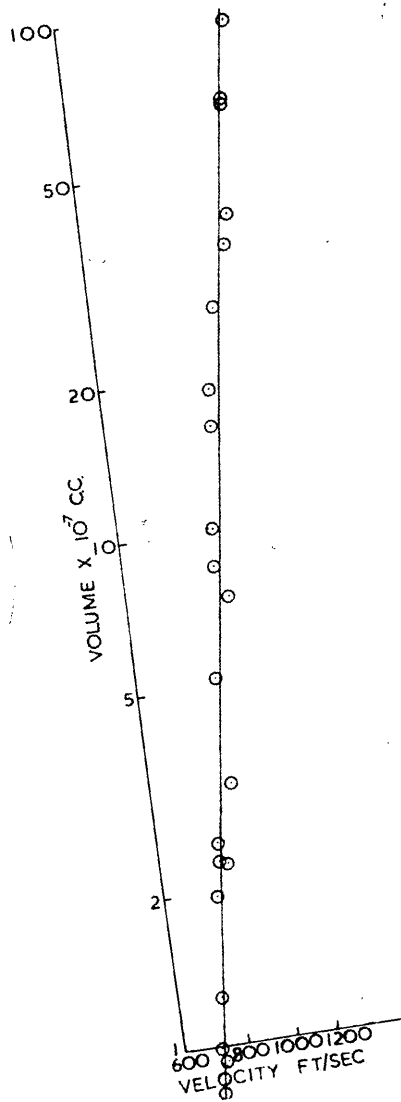
FIG 12.5

extreme edge of the circle of cracking. The profile of a crack, in which the surface pile-up is of this order of magnitude was shown in Chapter 10. The raising of the surface level may be due to the sides of the cracks being pressed together on removal of the tensile stress which produced the crack. These raised up regions will have a large torque exerted on them by flow of material on them, and thus material may be broken away from the surface. This however occurred in only one or two cases with impacts of polythene, as compared with all the higher velocity water drop impacts. (This may be due either to the lower flow velocity, or to the fact that flow had ceased by the time the cracks were formed). One specimen had been impacted with many pellets during the trial runs which had to be carried out to arrive at the best arrangement for ensuring that the pellets struck the impacting surface perpendicularly. Several regions could be seen where the damage sites overlapped, in some cases 3 or 4 cracked regions were intermingled. The general appearance was similar to that of the overlapping regions observed on the whirling-arm specimen (Chapter 14). A roughening of the surface occurred at the overlap causing the surface to act as a diffuse reflector, no surface breakup was observed however though there were many small squares of material surrounded by cracks. It had been envisaged that examination of up to about 6 overlaps in stages might give useful information though observation of the later stage might prove difficult. It would be more

satisfactory to experiment with actual rain drops, since, as
we have seen, little surface breakaway occurs with polythene
as compared with water drops.   If however the examination is
to be made after each impact, alignment would cause trouble.
Another possibility is to fire at several drops in a row.   In
this case only the end-product can be examined and it will be
similar to that obtained from the whirling-arm test.   Some
further work on these lines is desirable.

The depth of the cracks could be measured by sectioning
and using the technique described in Chapter 8.   This was
done on two specimens, one at 1,260 ft./sec. and the other
760 ft./sec.   The maximum crack depths were 87.5μ and 48μ The
cracks were perpendicular to the surface.   Time did not permit
the examination of more specimens, but it would be interesting
to see how the depth depended on the impact velocity, from the
point of view of the energy required to form a crack.   The
work of Bartoe (1943) has been mentioned previously.   He
found a reduction in impact strength in the presence of surface
scratches, but a marked difference occurred only for cracks of
depth   0.025 in. - 0.6 m.m.   He does not discuss the shape
of the scratches however, and probably the assumption that
they are infinitely thin does not hold.   Further work would
be desirable on this topic.

12.5 CONCLUSIONS

The rate of increase of the size of the damage site with

velocity has been determined and shown to be much greater than that occurring in impacts with a non-deformable solid. The nature of the damage is very similar to that occurring in raindrop impact, as is the size variation. The effect of the wash on the surface breakup at the cracks is however much less than in water drop impact.

12.6 IMPACTS ON DURALUMIN

The material used for the specimen was cut from the same bar as that used for the steel ball impacts. The surface was polished with alumina in water on a rotating Selvyt lap. A really good polish seems to be difficult to obtain on Duralumin but was good enough for the present measurements to be carried out. Pellets were fired at various velocities up to a maximum of 1,250 ft./sec., the velocity range was rather restricted however as the minimum velocity at which an easily detectable and measurable depression was produced was about 1,000 ft./sec.

The reflectivity of the Duralumin surface was high enough to obtain good reflection Fizeau fringes. Fig. 12.6 shows a Fizeau interferogram of the indentation. It can be seen that it is a fairly symmetrical shallow depression. The symmetry was not of the same order as that of a steel ball impact, since the polythene pellets were not true hemispheres and sometimes hit slightly skew. The results are however, of sufficient accuracy to show the rate of increase of the size of
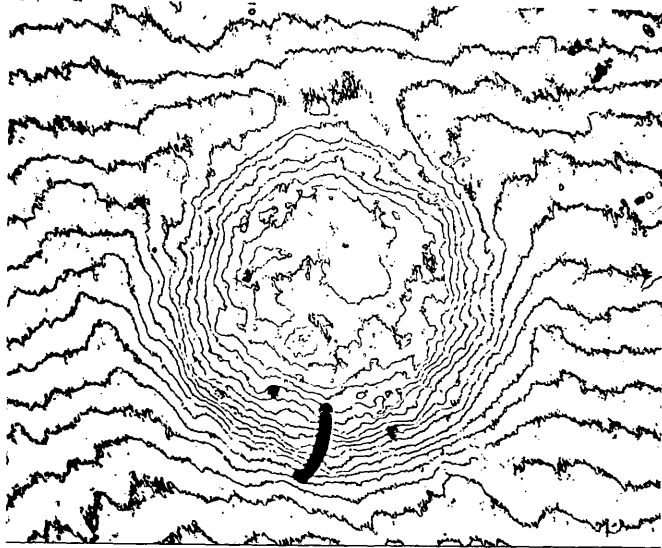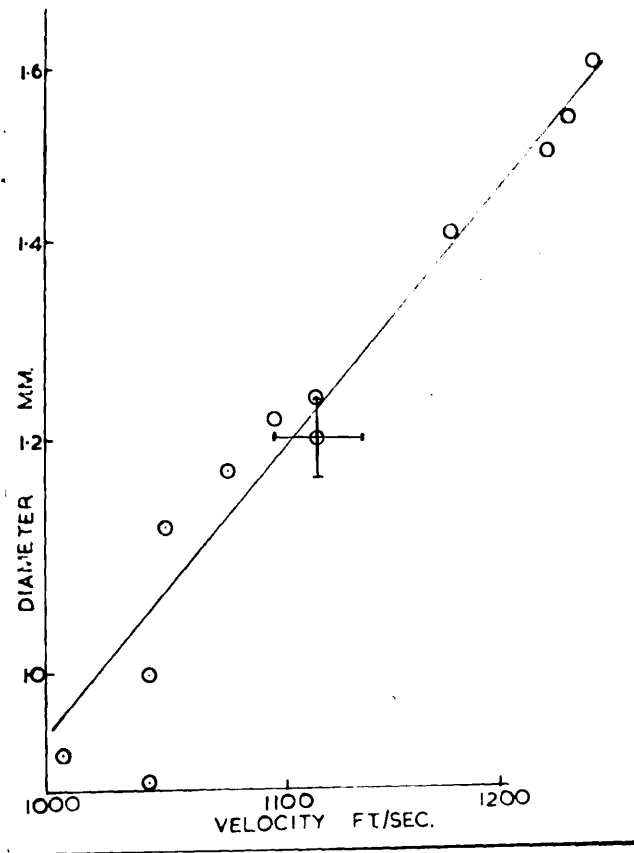
FIG. 12.6   1235 FT./SEC.   X 31

FIG. 12.7

the damage site with velocity, and are given in Table 6.

The diameters of the depressions were measured from the interferograms and plotted against the velocity, fig. 12.7. There is some scatter of the points since the error is fairly high both in diameter and velocity. The range of the error involved is shown on one point at about 1,100 ft./sec. The error in the diameter is due mainly to the factors mentioned above, the non sphericity of the polythene pellet and the tendency to hit slightly skew. The velocity error arises at the higher velocities measured since the time measured becomes rather short for the scale of the chronotron. This could not be increased by using a larger distance between the photo-cells since it would increase the tendency for the pellet to yaw. More precise experiments could be made if polythene spheres of higher quality could be moulded, and/or a timer registering times of the order of μ secs. was obtained.

The straight line shown in fig. 12.7 gives the law

$$d = kv^{2.3}$$

where $k = 1.41 \times 10^{-7}$, if d is in m.m. and v in cms./sec.

12.7 SHAPE OF THE INDENTATION

From the interferogram the shape of the indentation can be obtained. The usual Newtons ring formula for circular fringes of equal thickness is applicable if the indentation is a shallow one. The equation is

$$\delta^2 = 4n\lambda R$$

where δ is the diameter of a fringe, n the order of interference, and R the radius of curvature of the indentation. Thus if the depression is exactly spherical, plotting δ^2 against n would give a straight line, and the radius of curvature can be determined from the slope. This curve was plotted for several of the indentations. They were not truly spherical, but were approximately so, consistent with the degree of uniformity of the impactor. This essential sphericity is of importance since it gives information about the pressure distribution of the force deforming the surface.

The Hertz analysis shows that there is only one pressure distribution which will deform a flat surface into a portion of a sphere. This distribution is shown in the full line in fig. 5.4. The distribution for plastic deformation obtained by Ishlinsky is shown in the broken line. Thus there is a close similarity in the stress distribution involved in both elastic and plastic deformation. Hence on removal of the load, the elastic stresses are released and deform the indentation into a spherical surface of different curvature. This close similarity between the stress distributions is why the recovered indentation remains spherical.

The fact that a spherical indentation occurs in the case of polythene impact implies that the pressure distribution is as described above. Thus the indentation process occurring in the material is the same as if it were due to a load applied on a rigid sphere.

The radius of curvature of the indentation can be determined from its measured depth and diameter from the formula $R = d^2/8h$, if it is assumed to be spherical. (This is equivalent to assuming that the curve obtained by plotting n against δ^2 is a straight line passing through the points 0, and d^2, h). R varied between about 10 and 14 cms. increasing with decreasing velocity, which is very large compared with the radius of the nose of the undeformed pellet = 2.5 m.m. There are two reasons why a large value would be expected. The pellet will deform on impact, and the indentation is very shallow and in the elastic-plastic range where the elastic recovery will be very large and thus increase the radius of curvature. In experiments with steel ball indentors and very light loads, the radius of curvature of the indentation may be 5-10 times that of the indentor. A term shallowing is usually defined to denote the change in the depth of the indentation on recovery. This is defined as

$$S = \frac{h_o - h}{h_o} = 1 - \frac{h}{h_o}$$

where h_o is the depth of the indentation at the end of impact (i.e. before elastic recovery) and h is the depth of the recovered indentation. h can be measured directly from the interferogram as above. h_o is calculated from the diameter of the indentation and the radius of the ball, assuming that (a) the change in the diameter of the indentation on recovery is negligible, (b) the indentor is not deformed during the

VOLUME x 10⁻⁷ C.C.
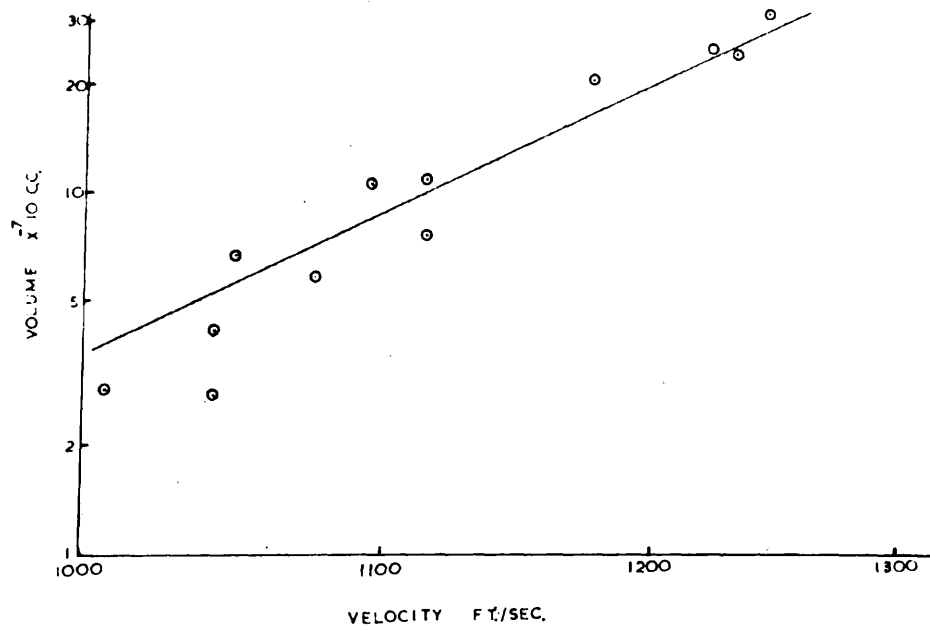
VELOCITY F T./SEC.

FIG. 12.8

impact.   Assumption (a) is usually assumed to be true within
a few per.cent but in the case considered a large deformation
of the indentor is involved.   Thus no estimate of the shallow-
ing could be obtained, other than the determination of the
radius of curvature.   The volume of the indent was calculated
from the formula

$$V = \frac{\pi d^2 h}{8}$$

where h = the depth and d the diameter of the indentation.
The variation of the volume with velocity is shown in fig. 12.8,
the graph yielding the law

$$Vol. = kv^{9.7}$$

Thus a very rapid increase in the volume of the indentation
occurs.   This is to be expected from the rapid increase in
diameter already noted.   The results must be interpreted with
some caution in view of the restricted range of velocities used,
and the fact that the indentations are elastic-plastic and
subject to shallowing.   In spite of the errors involved,
however, it is evident that an extremely rapid increase in the
amount of damage occurs.on increasing the impact velocity.

12.8 PRESSURE EXERTED OVER THE INDENTATION

The mean pressure required to initiate plastic deformation
was determined in Chapter 11.   This enables an estimate of the
pressure developed by the polythene sphere impact to be obtained

The minimum velocity needed is about 1,000 ft./sec.   If
we calculate the pressure assuming the polythene behaves as an

incompressible fluid we have, taking the density of polythene as 0.92

$$p = \rho v^2 = 0.9 \times (3.05 \times 10^4)^2 \text{ dynes/sq. cm.}$$

$$= 8.4 \times 10^8 \text{ dynes/sq.cm.}$$

From Chapter 11, the mean pressure for yielding $= 1.1Y$

$$= 5.6\text{-}6.4 \times 10^9 \text{ dynes/sq.cm.}$$

Thus the above expression gives much too low a pressure. If we use the Engel (drop)theory we have,

$$p = \tfrac{1}{2} \, 0.9 \rho c v$$

as the peak pressure. This gives an appreciably higher result but the difficulty is that the value of the velocity of sound is not known for the conditions of the experiment, as it varies with the frequency. Hillier (1949) measured the velocity of rod waves and showed that the rate of increase is small at the higher frequencies (as would be expected for the model described in Chapter 2). His value is 1×10^5 cms./sec. The velocity of dilatational waves will be greater than this, depending on the Poisson's ratio of the material. The value is not known, but will be large since the shear modulus of polythene is small, (Kolsky 1956). The velocity (c_1) of dilatational waves is given by

$$c_1 = \left\{ \frac{E}{\rho} \, \frac{(1-\sigma)}{(1+\sigma)(1-2\sigma)} \right\}^{\frac{1}{2}}$$

and thus becomes much larger than $(E/\rho)^{\frac{1}{2}}$ when σ approaches 0.5. If we assume $\sigma \doteq 0.4$ say, then $c_1 = 2(E/\rho)^{\frac{1}{2}}$, this is probably a minimum value. Then we have

$$p = 0.45 \, \rho v c = 2.5 \times 10^9 \text{ dynes/sq.cm.}$$

This is still too low but gives a better value than from the previous method.   It is evident that some type of flowing deformation is occurring at this velocity, which is below that required for fluid flow, similar to that discussed for metals by White and Griffis (1948).

12.9 SHAPE OF THE PELLET

At the highest velocities used, the pellet is deformed to about 1½ times its original diameter.   The interesting point is that the impacting surface is highly concave.   This indic- ates that wave phenomena are occurring in the pellet and in the pellet and the concavity is probably due to the reflected tensile waves from the free end.   Lee and Tupper (1954) analysed the reflection occurring when a flat ended metal cylinder is fired at a rigid target, for one particular velocity of impact.   They show that the particle velocity in the plastic wave front is gradually distroyed by the reflected elastic waves.   This explains why the plastic front only penetrates a certain amount.   In the present problem with spherical surfaces the analysis is correspondingly more com- plicated, but this gives a qualitative explanation.

12.10 SURFACE PITS AND ROUGHENING

A feature of several of the indentations was the presence of a small pit near the centre of the depression.   This was usually about 1μ deep and about 0.005 m.m. diameter. Presumably they are initiated at small pits already present on

the surface, and pressure multiplication can occur due to
their conical shape. An annular region where the surface
was roughened by the wash, was seen on many of the impact
sites. The region was inside the rim of the indentation,
and seems to coincide with the position of the annular de-
pression obtained on Perspex. This indicates a possible
heating effect due to the flow.

12.11 SIMULATION OF RAINDROP IMPACT

Since the nature of the damage produced by polythene
spheres and raindrops appears to be similar, it may be
possible to use the spheres to simulate raindrops.

The chief difficulty which arises is that of knowing
what features of raindrop impact we wish to simulate (for the
purpose of assessing the durability of materials to rain
erosion). If it is desired to assess the material in terms
of the size of the indentation formed at a given velocity it
seems that the polythene sphere test should be of value.
Thus from the equations obtained for the polythene impact
process, knowing the constants given, it should be possible to
calculate the size of a raindrop impact. Not enough data has
been obtained in the present work however for this calculation
to be made, as the effect of the size of the drop (or pellet)
has not been studied. In solid sphere impact, the diameter
of the damage site is directly proportional to the radius of
the ball. This assumption cannot be made in liquid sphere
impact and further work must be done both with polythene and
waterdrop to assess this before a simulated test can be used.
It may be difficult to make polythene spheres of the same size
as the largest raindrop, and hence extrapolation will be
necessary.

TABLE 6

Vel. ft./ sec.	Dia. of Depression m.m.	Log. Vel.	Log. Dia.	Vol. of Depression $\times 10^{-7}$c.c.	Log. Vol.
1007	0.94	3.0030	.972	2.83	.452
1042	0.92	3.0179	.963	2.72	.436
1042	0.98	3.0179	.990	4.14	.617
1049	1.12	3.0208	0.049	6.71	.827
1076	1.17	3.0318	0.068	10.72	1.030
1096	1.22	3.0398	0.086	5.88	.769
1116	1.20	3.0476	0.079	7.72	.888
1116	1.24	3.0476	0.094	11.50	1.047
1178	1.41	3.0712	0.149	21.3	1.328
1225	1.50	3.0881	0.176	26.4	1.422
1235	1.54	3.0917	0.187	25.5	1.407
1248	1.61	3.0962	0.207	33.4	1.524

CHAPTER 13

IMPACTS ON WATER DROPS

13.1 INTRODUCTION

The specimen, in the form of a short flat ended cylinder, was fired at a water drop suspended on a chemical web.   Jenkins 1955.   The web is stretched across a hole drilled in a cork and is formed from a mixture of Perspex dissolved in Aniline.   A drop diameter of 2 m.m was chosen. The volume of a drop of this size was calculated, and measured out using an "Agla" micrometer syringe.   One division of the micrometer screw corresponded to 0.2 c.m.m.   The diameter of the drop placed on the web was measured in two directions at right angles using a travelling microscope.   This was repeated for about 5-6 drops and results were consistent, although some distortion of the drop occurred.   Ideally the gun should be mounted vertically so that the web is horizontal. To stop the specimen after impact a tube filled with pads of cotton wool, placed about 1 in. apart was mounted behind the dre This slowed down the specimen without appearing to cause any damage, although care had to be taken to ensure that each pad was lightly packed.

The barrel diameter was nominally 0.265 in.   The specimens were turned up slightly undersize and it was necessary to cut grooves in the end so that the specimen did not yaw.
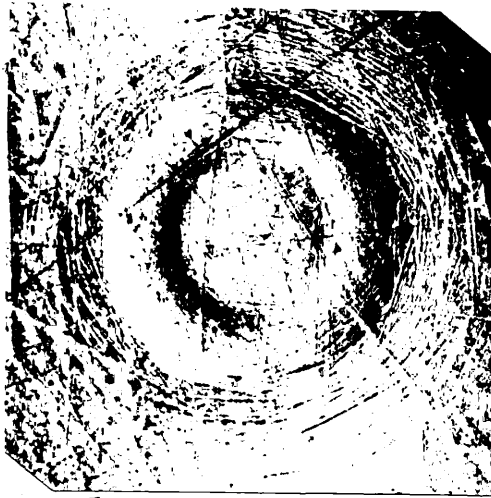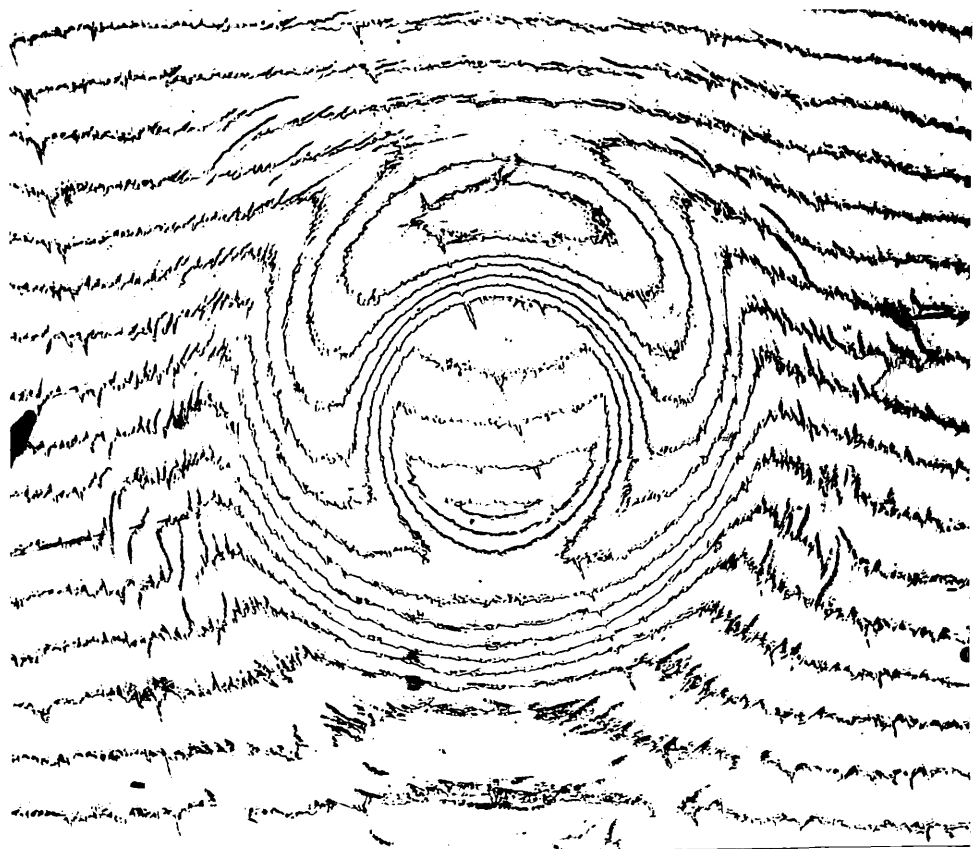
Fig. 13.1   X46

Fig. 13. 2   1060 Ft./sec.   X68

The minimum specimen mass was of theorder of 200 m.g., the drop mass = 4 m.g, so that any change in velocity due to momentum transfer would be small.   In any case the indentation may occur during the first stages of impact before the whole mass of the drop has been set in motion.   No allowance has been made for the effect of the web.   The fact that a symmetrical impact site was obtained suggests that it is blown away from the drop by the air blast preceding the projectile.

13.2 PERSPEX CYLINDERS

The striking surface was ground and polished with I.C.I. Perspex polish giving a very good finish.   Specimens were fired at various velocities up to a maximum of about 1100 ft./sec They were then silvered and examined microscopically.   The damage consisted of a very shallow indentation at the centre bounded by an annular depression which is surrounded by a region of fine cracks.   It is similar to the damage produced by polythene impact.   It differs in that the fine cracks are predominantly straight, though some are short and curved. There is some evidence that this tendency towards straight cracks is due to polishing of the surface, as mentioned for steel ball impact.   Polythene spheres were fired at a polished surface, the number of straight cracks appeared to increase, but the shorter irregular type still predominated.   The general nature of the damage can be seen in Fig.(13.1), it was taken with obliquely reflected illumination.   The Fizeau interferogram fig.(13.2) shows the depth of the depression and
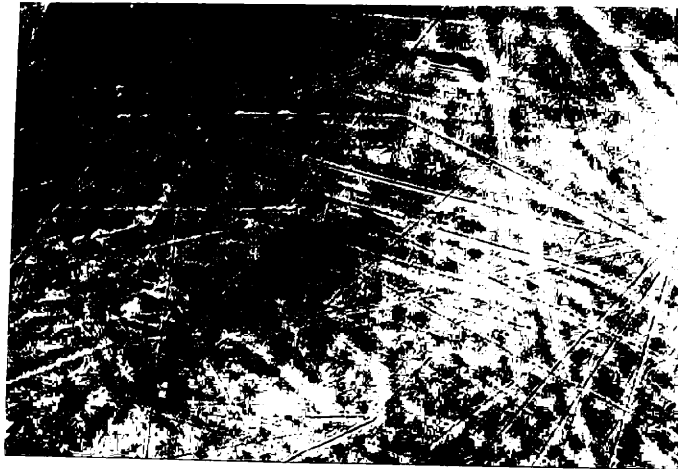
FIG. 13. 3   X 170
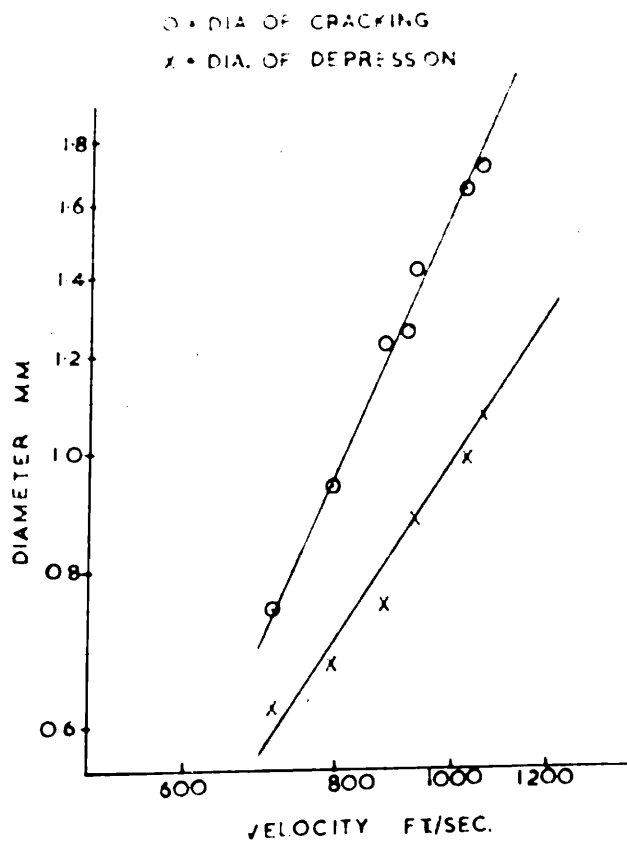

O = DIA. OF CRACKING
X = DIA. OF DEPRESSON

FIG 13.4

the surface displacements at the surrounding cracks.
Fig.(13.3) shows the breaking away of material from the
outer edge of the cracks due to the rapid radial flow of
water.

A similar deformation mechanism to that postulated in
polythene impact is put forward to explain the presence of
the fine cracking. The measurements made are shown in
Table 9.

As before, the diameter of the cracked region was
plotted on a log-log scale against the impact velocity, giving
a linear relationship: Fig.(13.4) $d = kv^{2.2}$
where $k = 4.5 \times 10^{-7}$, d is in m.m. and v in ft./sec.
The diameter of the depression was also plotted and the
relation $d = kv^{1.5}$
obtained, where $k = 3.37 \times 10^{-5}$, Fig. (13.4).

A section of the surface was plotted from the interfero-
gram and is shown in Fig.(13.5), with the profile of a drop
inserted for comparison. The volume displaced by the
depression was calculated from the internal and external
radii and the depth, again making the assumption that it is
of trapezoidal section, the error involved being small. A
plot of volume against velocity yields a law of the form
$Vol = kv^{8.2}$ (Fig.13.6). The rate of increase with velocity
is thus similar to that occurring in polythene impact.

The main differences between the damage sites produced
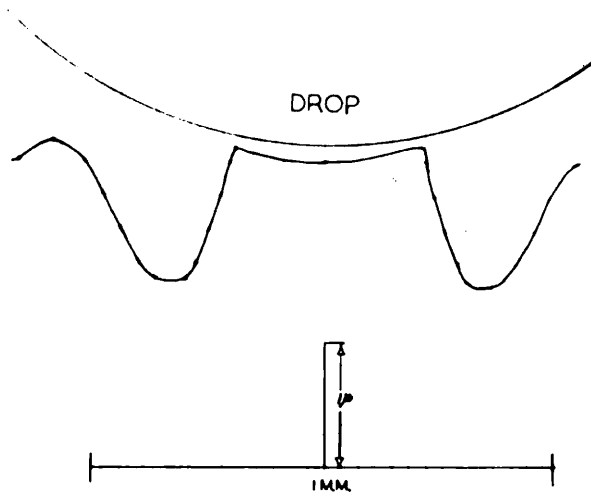by a water drop impact and by polythene can be summarised as

DROP

1MM.

FIG. 13.5

VOLUME X 10⁻⁷ C.C.

4·0
2·0
1·0
0·8
0·6
0·4

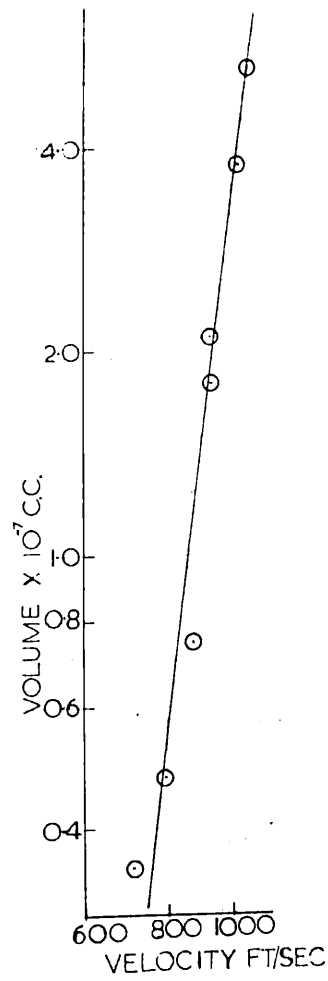600 800 1000
VELOCITY FT/SEC

FIG. 13·6

follows.   The tendency for fewer but longer straighter cracks to occur, and considerably less roughening of the surface in the region of the annular depression.   No region where the Fizeau fringes ∕ [were] completely broken up occurred as was observed for polythene but the maximum velocity attainable in water drop impact was lower because a short cylinder of the material had to be accelerated.   That surface displacements of the order of 0.1 in occur at the cracks can be inferred from the interferogram and as shown in Fig.(13.3), material may be broken away at these points.

13.3 ALUMINIUM CYLINDERS

The original idea had been to cut specimens from the same bar of Duralumin as was used for the steel ball and polythene sphere impacts, so that a direct comparison could be made. The maximum velocity attainable however was about 1000 ft./sec. which was only just sufficient to produce a depression on the Duralumin.   Thus to enable a series of impacts to be made at varying velocities, aluminium was used, being considerably softer than Duralumin.   The drop size used was 2 m.m. diameter as before.

Impacts were made at velocities in the range 700 ft./sec.- 1000 ft./sec.   Each damage site consisted of a spherical Brinell type depression.   Some roughening of the surface is apparent inside the indentation over its edge.   This is probably due to the flow of liquid up the sides of the depression.   All the impact marks were single and symmetrical
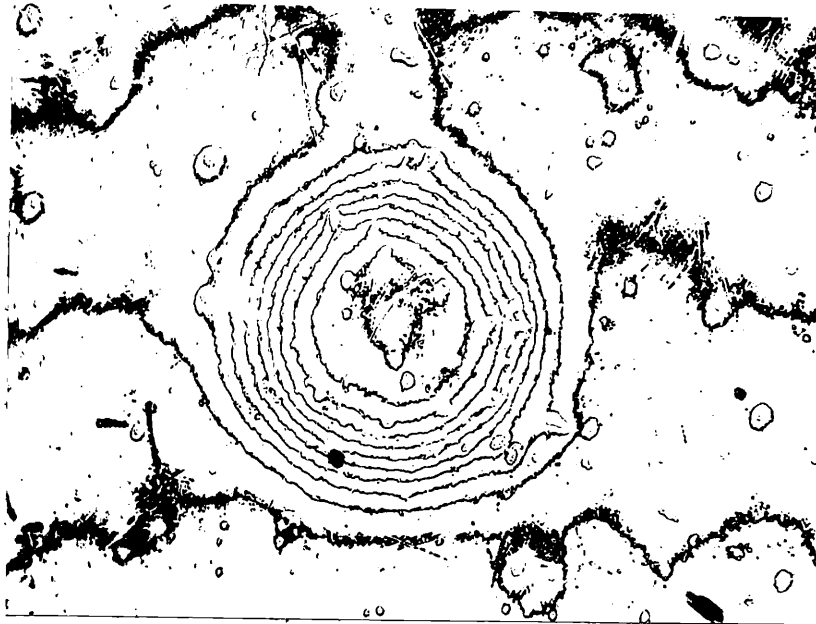
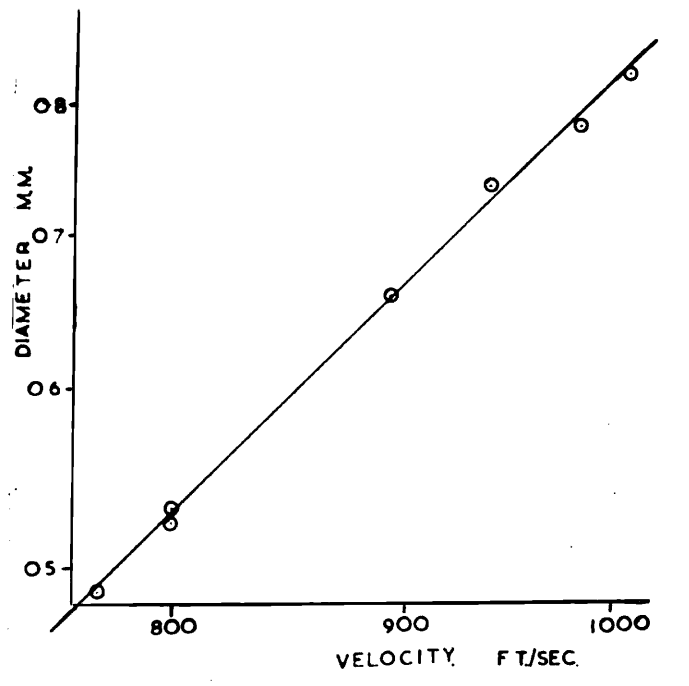FIG. 13.7   1000 FT./SEC.   X62

FIG. 13.8

showing that the drop had retained its shape on impact,
i.e. it is behaving similarly to a hard sphere.   A Fizeau
interferogram of a typical indent is shown in Fig.(13.7).
From the interferograms the diameter of the depression was
measured, as seen in Table ¨8.¨.   On plotting this against
the velocity (log.log. scale) a straight line graph was
obtained giving the experimental law

$$d = kv^{2.0}$$

where $k = 9.4 \times 10^{-7}$ when d is in m.m. and v in
ft./sec. Fig.(13.8)

The scatter of the points is much less than in the
experiments with polythene, due mainly to the fact that the
drop shape and size could be more precisely controlled than
the striking surface of the polythene pellet.   The somewhat
lower velocity used also reduces the error somewhat.

The shape of the indentations was roughly spherical, as
determined by a plot of the square of the diameter of a
fringe against the firing number as described in Chap (12).
From the interferograms the depth(h) can be determined and
the volume of the depression calculated from the formula
$Vol = \pi d^2 h/8$.

Plotting volume against velocity on a log.log. scale
gives the relation, Fig.(13.9)

$$Vol = Const. \ v^{8.9}$$

Thus the law connecting the size of the impact site with
velocity is similar for polythene and water drop impact on
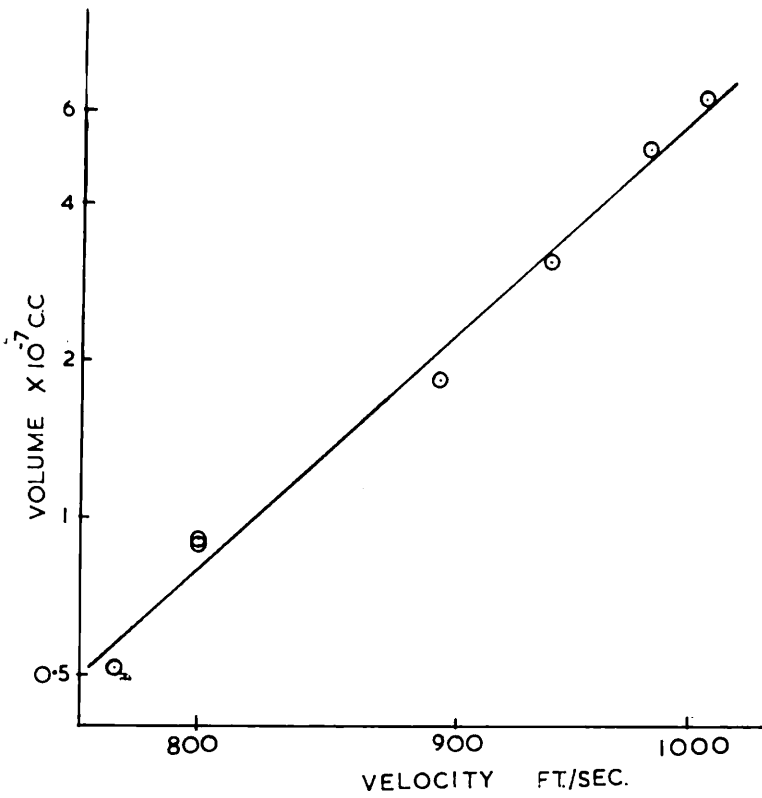metals as well as on plastics.

FIG. 13. 9

13.4 SHAPE OF THE INDENTATION

As stated above, the indentations can be regarded as approximately spherical in shape. The radius of curvature (R) is much larger than the radius of the drop for reasons similar to those discussed in Chapter 12. R varied between 3.5 and 5.5 cms. depending on the velocity.

13.5 PRESSURE DEVELOPED IN IMPACT

The hardness of the aluminium specimens was measured using a Brinell type of test. The mean value obtained for the Meyer Hardness was 40 Kg/sq.mm.

Hence the mean pressure pn required to initiate plastic deformation under static conditions is

$$= 1.1Y \text{ where } Y = \text{the Yield Stress}$$
$$= \frac{40}{2.8} \times 1.1 = 15.7 \text{ Kg/m}^2$$

Thus $p_m = 1.54 \times 10^9$ dynes/cm^2
= Mean Pressure

This is for the static case. It was stated in Chapter 11 that the dynamic yield pressure of Duralumin was about 20% greater than the static value. The minimum difference between the static and dynamic values of the yield pressure of Aluminium would be of this order.

Thus the Mean Pressure = 1.85×10^9 dynes/cm^2.
We compare this with the value obtained for the pressure from the Engel equation. (Though this is actually the maximum value of the pressure.)

We have,   pressure $= \frac{1}{2} \alpha \rho c \, v$

$\alpha = 0.9$, c = velocity of sound in water = 1500 metres/sec.

$\rho = 1$, Minimum impact velocity required for damage to occur
$$= 700 \text{ ft./sec.}$$

Hence the pressure $p = 0.45 \times 1500 \times 2.14 \times 10^4$
$$= 1.45 \times 10^9 \text{ dyns/cm}^2.$$

This value is somewhat low but of the right order of magnitude. The discrepancy between the theoretical and practical values could be due to either a wrong expression for the pressure, or that a higher value of the velocity of sound than the normal one occurs due to the shock loading. Possibly a combination of the two is involved.

TABLE 7

Vel. ft./sec.	Dia. of Cracking m.m.	Dia. of Depression m.m.	Vol. of Depression x10^{-7}c.c.
710	.744	0.620	0.351
795	.937	0.670	0.473
878	1.23	0.750	0.745
918	1.26	0.893	1.79
932	1.42	0.882	2.10
1024	1.65	0.992	3.79
1060	1.73	1.07	5.28

TABLE 8

Vel. ft./sec.	Dia. of Indent m.m.	Vol. of Indent x10^{-7}c.c.	Log. Vel.	Log. Dia.	Log. Vol.
771	0.489	0.513	2.887	0.689	0.710
800	0.524	0.885	2.903	0.719	0.947
800	0.532	0.910	2.903	0.726	0.959
892	0.659	1.861	2.950	0.819	1.270
938	0.737	3.145	2.972	0.867	1.498
982	0.784	5.26	2.992	0.894	1.721
1007	0.827	6.59	3.003	0.917	1.819

CHAPTER 14

MULTIPLE DROP IMPACT

A whirling arm technique is used ▬▬▬▬▬▬▬▬, (R.N.C.
Strain. 1955) as a simulated test for the rain erosion of
.materials.   The specimens are attached to the ends of the
arm which is rotated in a region of artificial rain.   This
is produced by the spinning disc technique (Walton & Prewett,
1949), in which the drop size can be controlled by the
diameter and velocity of the disc.   A test speed of 500 mph
(733 ft./sec.) is used.   The specimens are in the form of
hollow cylinders and are mounted with their axes at right
angles to the arms.   Thus a constant velocity of impact is
achieved along the whole length of the cylinder.

In order to compare results obtained with single drop
impact tests with those from this simulated test, a "Perspex"
specimen was subjected to 1 in/hour rainfall for one minute.
This short time of exposure ensured that the marks due to
separate impacts could be distinguished.   The eroded area is
confined to a narrow strip along the leading edge of the
specimen.   To the naked eye, the damage appeared to consist
of a general roughening and pitting of the surface causing a
loss in transparency.

The area to be studied was silvered and examined micro-
scopically Fig.(14.1), showing that the surface roughening
consisted of many impact marks similar to those observed in
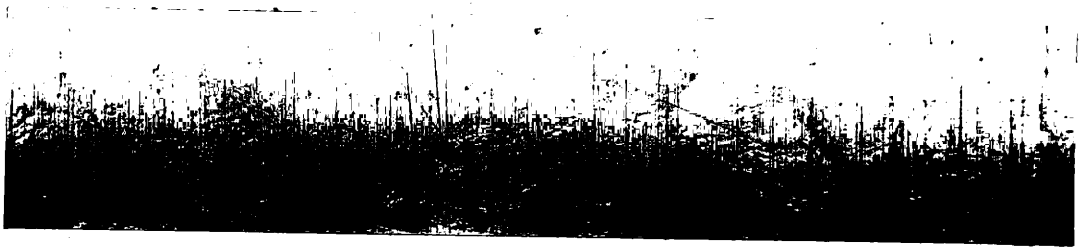
FIG. 14.1   X 12

the single drop technique. Each annular depression is surrounded by fine cracking and material is broken away from the edge of the cracks. The cracks are difficult to see due to the overall surface roughness (turned surface), but appear to be less regular than those observed with the single drops, and similar to the shorter cracks produced by polythene spheres. This difference may be due to the surface roughness and the fact that the material is not polished as mentioned previously. Considerable breakaway also occurs along the turning marks and hence the surface finish will be an important factor in determining the initiation of damage.

The diameters of the depressions were in the range 0.7 - 1mm. The velocity of the specimen was 733ft./sec. and the median volume diameter of drops in 1in/hr rain is given as 2.4mm. This compares with a diameter of about 0.7mm. obtained by the author with a 2mm. drop impact at a similar velocity. No measurement of the depth of the depression was made as the surface was too rough for interferometric study.

In some regions the cracks of adjacent impact site. overlapped. Damage occurred due to the wash, but it is not easy to decide whether it was more pronounced here than elsewhere. It would be of considerable interest to study the breakup process on specimens tested for, say, 1 min. or ½ min. increments to see whether it is initiated more rapidly at the overlap.

Summing up it can be said that the impact marks

obtained by both methods of test are similar, so that

conclusions reached from single drop tests are v li for

the multiple case.   The damage falls off very rapidly as

one moves away from the leading edge, and a good surface

finish may delay the initiation of damage due to the wash

of the drop.

CHAPTER 15

THE EFFECT OF TEMPERATURE
ON THE NATURE OF THE DAMAGE TO PERSPEX

15.1 INTRODUCTION

When a "Perspex" specimen is impacted with a relatively soft spherical impactor, the nature of the damage site is as shown in Fig.(13.5). This annular depression does not occur in steel ball impact.

If the impacted specimen of Perspex is heated up to about 120°-140°C for about ½hr., the depression recovers. This indicates that the depression is not formed by removal of material by the wash effect but is a frozen-in high elastic deformation.

We can describe the mechanism of retarded elastic deformation by a Voigt Element, as discussed in Chapter 2.

$$\text{The strain } \epsilon = \frac{S}{E_2}(1-e^{-t/\lambda})$$

Thus the strain is a function of both the stress and the time of impact. If $t \ll \lambda$ say $t = \lambda/100$, then

$$\epsilon = \frac{S}{E_2} \cdot \frac{1}{100}$$

so that the stress required to produce a given strain can be large if the time of impact is small compared with the relaxation time. The value of the relaxation time is reduced by increasing the temperature, so that high elastic deformation might occur if the temperature was increased.

This would be "frozen-in" since the stress available for recovery depends only on ϵ and E_2 and will be much lower than the deforming stress.

If the temperature is raised sufficiently, however, so that $\lambda \approx t$, the deformation would be recoverable within the timescale of the experiment.

Thus from the equation overleaf, for deformation to occur in an annular region, two possibilities emerge: either (a) The value of t must be larger here than in the rest of the impact site (and larger than in steel ball impact). A simple increase in the value of the stress in the region is ruled out by the spherical nature of the depression in a metal. and/or (b) The surface temperature must be increased in the annular region due to the wash. Rapid flow will occur here under considerable pressure since the annulus is inside the main area of elastic compression.

Some support for mechanism (a) is provided by the nature of the stress-time distribution in liquid drop impact, the reduction in pressure at the centre of the impact site due to the arrival of a focussed tensile wave.

Evidence for a possible local temperature rise is provided by a surface roughening which appears in an annular region, in impacts with water drops or polythene pellets on Perspex and aluminium. Bowden and Tabor (1956) state that very high surface temperatures are reached when solids of low thermal conductivity slide on one another. Since

contact occurs in a few regions only, the high temperatures are localised and the bulk temperature change is small.

15.2 EXPERIMENTS AT VARIOUS TEMPERATURES

Experiments have been made with the Perspex specimen at various temperatures and the results are shown in Table 9. The temperatures given are very approximate but are considered to be sufficiently accurate to show the trend of the deformation.

For the high temperature experiments the specimen was heated in an oven, quickly removed, mounted between two corks and impacted. The cooling was achieved by immersing in liquid air and proceeding as before.

TABLE 9
Nature of Damage Site

Impactor	Room Temp	130-140°C	-100°C apy.	+90°C
Steel Ball	Circle of Crazing. No Permanent deformation	Circle of crazing. As at room temp	Crazed circle As at room temp	Crazing + permanent spherical deformation
Polythene Ball	Annular depression surrounded by crazing.	Crazed region. Very slight spherical depression.	Crazed region and annular depression.	Crazed region and annular depression.

All "permanent" depressions disappear on heating to 140°C for ½hr. At room temperature, however, the deformation seems to be completely "frozen-in". A specimen fired at a water drop has been remeasured 130 days after the original measurement and no appreciable change was observed. This indicates

that the relaxation mechanism must be non-linear under the
high strain rate during impact.

15.3 DISCUSSION

The results obtained with the steel ball, that is, the
spherical depression produced when the specimen is at -90°C,
and its disappearance at a temperature of 140°C are as pre-
dicted from the equation for the Voigt element.

When using the polythene sphere, the effects at 140°C,
i.e. the recovery of the high elastic deformation, is as
expected. It is not possible, however, to distinguish between
effects due to a change in the stress distribution and the
heating effect of the wash, both factors probably contribute.
The occurrence of the annular depression at 90°C is a point
in favour of a change in the stress distribution. The
thermal conductivity of Perspex is low, (1.5 x 10^{-3}
joules /cm/sec/°C), the specific heat is 0.35 and density is
1.19 gms/c.c.

The thermal properties of polythene are similar to those
of water, the thermal conductivity of polythene is 3.4 x 10^{-3}
and of water 6 x 10^{-3} joules/cm/sec/°C. The specific heat
of polythene is 0.6, and density 0.92

The volume of the depression formed in Perspex is of the
order of 10^{-6}c.c. so that the amount of heat required to
cause a local rise of temperature in that region is small.
This fact, together with the low conductivity, strongly

suggests a mechanism of local heating. Since the volume is small this could occur even at the lowest testing temperature when the surface of the specimen is covered with a frozen layer of condensed water vapour.

It would be interesting to measure the possible temperature rise. It might be feasible to observe this using a sensitive infra-red detector, but the short rise-time would cause difficulties, and the cut-off wavelength of Perspex is about 2.7 μ.

CHAPTER 16

DISCUSSION OF RESULTS

The theories of drop impact discussed previously, do not give any idea of the variation in size of the damage site with a change in the velocity of impact.

In order to be able to get an estimate of this variation it seems to be essential to consider the two halves of the problem separately. Normally, in solid-solid impact the system is considered as a whole, and the relation between the diameter of the indentation and the velocity is obtained. In the case of a liquid drop, two factors are operating, the variation of the diameter of the indentation with the force, and the variation of the force with velocity. Thus the force on the surface due to the impacting water drop is a function of the velocity, and the size of the resulting damage site will be a function of this force.

Consider the instant when the material is at its maximum deformation. The force producing the deformation is balanced by the reaction due to the elastic forces in the medium. Examination of both the polythene and water-drop indentations on Aluminium reveals that they are essentially spherical depressions. Thus as far as the material is concerned, to a first approximation, the deformation can be considered to be produced by a force distributed on the surface such as to produce a spherical depression. It is well known (Hertz 1896), that only one distribution of pressure will deform a flat

surface into a portion of a sphere. Thus we can use the relation between the force applied and the diameter of the indentation as derived from Hertz theory. We had

$$P = k\alpha^{3/2} \qquad (1)$$

where α is the penetration,

and $\qquad 8R\alpha = d^2$

where R is the radius of the deforming sphere and d the diameter of the indentation. Thus

$$P = \frac{kd^3}{(8R)^{3/2}} \qquad (2)$$

Thus if to a first approximation R is considered constant, the relation becomes

$$P = K'd^3 \qquad (3)$$

This applies strictly to elastic deformation, and as some plastic deformation occurs we must write

$$P = K'd^n \qquad (4)$$

where n can very from 3 for elastic, falling to 2 for a fully plastic deformation. In the case considered only a small amount of deformation occurs and n should lie between 2.5 and 3.

The force F developed by the water drop can be written as $\qquad F = k'\rho A \, f(v) \qquad (5)$

where ρ is the density of the liquid, A the area of the surface deformed, $f(v)$ is some function of v,

or $\qquad F = k''\rho \, d^2 \, f(v) \qquad (6)$

Equating the force exerted by the drop and the reaction of the surface, we have, $\qquad F = P$

i.e.

$$K'd^n = k'' \rho d^2 f(v) \qquad (7)$$

$$d^{n-2} = K f(v) \qquad (8)$$

If the liquid is considered incompressible, as stated in Chapter 6, $f(v) = v^2$.

If we consider it compressible and apply the Engel theory,

$$f(v) = v.$$

Hence we can write

$$d^{n-2} = Kv^m \qquad (9)$$

$2.5 < n < 3, \quad 1 < m < 2.$

It was found experimentally that a relation of the type, $d = Kv^2$ described the impact in the velocity range considered. This relation can be obtained from the equation (9). Unfortunately, neither the value of n nor of m to be used is known accurately. Thus it is not possible from this equation to decide, which of the equations for the pressure exerted by the drop is valid.

The effect of the change in the radius of curvature of the indentation has so far been neglected. There are two factors which contribute to a change. The amount of elastic recovery taking place, which depends on the depth of the indentation, and the change in shape of the common surface of the drop and specimen at the time of maximum deformation. Both of these factors will tend to reduce the measured radius of curvature, as the velocity increases. This will increase the value of P for a given diameter, as shown by equation (2). Thus in equation (4) the effect is similar to an increase in

the exponent n. This factor will thus prevent the breakdown
of equation (9) when n $\longrightarrow$ 2 as it could do for a deep
indentation which would occur at a high velocity. If more
experiments could be made at higher velocities thus reducing
the effect of elastic recovery and the effective value of n
(in the case of a metal) it might be possible to decide the
value to be assigned to m. A direct method involving pressure
measurement Piezo-electrically is to be preferred, although
this presents great experimental difficulties.

From the comparisons made between the Yield Pressure of
the material and the calculated pressure using the Engel theory,
it is apparent that this approach gives the better result, but
the theoretical value is less than the pressure actually
developed.

R E F E R E N C E S

AIRY, G. (1831) Math. Tracts, 381.
ALFREY, T. (1948) Mechanical Behaviour of High Polymers
          Interscience.
BANNING, M. (1947) Jour. Opt. Soc. Amer., 37, 792.
BARTOE, W.F. (1943) Aviation, 42, 128.
BERGSMANN, E.B. (1954) Sheet Metal Ind., 31, 383.
BHIDE, V.G. (1956) PH.D Thesis, London.
BOULOUCH   (1893) J. de. Phys., 2, 316.
BOULOUCH   (1906) Jour. de. Phys. Rad., 5, 789.
BROBERG, K. (1956) K.T.H. Avhandl. No.111 Stockholm.
BOUSSINESQ, M.S. (1883) Compt. Rend., 97, 154.
BOUSSINESQ, M.S. (1893) History of Elasticity & Strength
          of Materials Vol.II. Todhunter & Pearson.
BOWDEN, F.P. and TABOR, D. (1956) Friction and Lubrication
          Methuen.
CAMPBELL, J.D. (1953) Jour. Mechanics & Physics of Solids,
          1, 113.
CAMPBELL, J.D. & DUBY, J. (1956) Proc. Roy. Soc. A.,
          236, 24.
CLARK, D.S. & WOOD, D.S. (1949) Proc. A.S.T.M., 49, 717.
CLARK, D.S. & WOOD, D.S. (1950) Proc. A.S.T.M., 50, 577.
COLE, R.H. (1948) Underwater Explosions Princeton.
CROOK, A.W. (1952) Proc. Roy. Soc. A, 212, 377
DAVIES, C.N. (1939) Unpublished M.O.S. report.
DAVIES, R.M. (1948) Phil. Trans. A., 240, 375.
DAVIES, R.M. (1949) Proc. Roy. Soc. A., 197, 416.
DONNEL, L.H. (1930) Trans. A.S.M.E. (J. App. Mechs), 52, 153.
DUFOUR, C. & HERPIN, A. (1954) Opt. Act. 1, 1.
ENGEL, O.G. (1953) Unpublished work.
ENGEL, O.G. (1955) Unpublished work.
ENGEL, O.G. (1955) Jour. Res. N.B.S., 54, 281.
FABRY, C. & PEROT, A. (1897) Ann. de Chim. et de Phys.
          12, 459.
FABRY, C. & BUISSON, H. (1919) Jour. de Physique, 9, 189.
FIZEAU, A.H.L. (1862) Compt. Rend., 54, 1237.
GRIFFITH, A.A. (1921) Phil. Trans., 221, 180.
               (1924) II Int. Cong. Appl. Mech. Delft.
HAAR, A. & VON KARMAN, T. (1909) Nachr. d. Gesellschaft d.
          Wissensch. zu Gottingen, 204.
HAIDINGER, W. (1849) Pogg. Ann., 77, 217.
de HALLER, P. (1933) Schweitz. Bauzeitung, 101, 243.
HAMY, M. (1906) J. de Phys., 5, 789.
HAWARD, R.N. (1945) Phil. Mag. (7) 36, 777.
     "   "   (1949) Strength of Plastics & Glass
          Cleaver-Hulme.
HEAVENS, O.S. (1953) Optical Properties of Thin Solid Films.
          Butterworth.
HENCKY, H. (1923) Z. Arg. Math. Mech. 3, 250.

REFERENCES - continued.

HERTZ, H. (1881) J. Reine Angew. Math., 92, 156.
          (1896) Misc. Papers. Macmillan, London.
HILLIER, K.W. (1949) Proc. Phys. Soc. B., 62, 701.
HITCHCOX, G. (1956) Electronic Engineering, 28, 298.
HOLDEN, J. (1949) Proc. Phys. Soc. B., 62, 405.
HONEGGER, E. (1927) B.B.C. Mitteilungen, 14, 95.
HOPKINSON, B. 1914 Phil. Trans. A., 213, 437.
HUBER, A. T. (1904) Czasopismo technczne, Lemberg.
HUNTER, S.C. (1957) Conf. Props. Materials at High Strain
          Rates. Inst. Mech. Engrs. 2, 5.
ISHLINSKY, A.J. (1944) J. Appl. Math. & Mech. (Leningrad)
          8, 233.
JENKINS, D.C. (1955) Nature, 176, 303.
    "   "   (1956) Private communication.
von KARMAN, T. & DUWEZ, P. (1950) J. App. Phys., 21, 987.
KOKADO, S. (1927) Tech. Repts. Tohoku Univ., 6, 201.
KOLSKY, H. (1953) Stress Waves Waves in Solids, Oxford.
    "   "   (1956) Phil. Mag. (8) 1, 693.
KOLSKY, H. & CHRISTIE, D.G. (1952) Trans. Soc. Glass.
          Tech. 36, 65.
KOLSKY, H. & SHEARMAN, A.C. (1949), Research, 2, 384.
KUHN, H. (1951) Reports on Progress in Physics, 14, 64.
LEE, E.H. (1957) Conf. Prop. Materials High Strain Rates
          Inst. Mech. Engrs., 4, 4.
LEE, E.H. & TUPPER, S.J. (1954) J. App. Mechs., 21, 63.
MAXWELL & HARRINGTON (1952) Trans. A.S.M.E., 74, 579.
von MISES, R. (1913) Nachr. d. Gesellschaft d. Wissensch.
          zu Gottingen, Math. Phys. Klasse 582.
MOHR, O. (1900) Zeits. d. Vereines Deutsch. Ingenieure 44, 1.
NADAI, A. (1931) Plasticity. McGraw Hill.
O'NEILL, H. (1934) Hardness of Metals. Chapman & Hall.
PASCOE, M.W. & TABOR, D. (1956) Proc. Roy. Soc. A., 235, 210.
PRESTON, F.W. (1927) Jour. Soc. Glass. Tech. 11, 283.
PROWSE, W.A. (1936) PHIL. MAG. (7) 22, 209.
RAKHMALUTIN, K.A. (1945) Appl. Math. & Mech. (Leningrad) 9, 1.
RAYLEIGH, Lord. (1906) Phil. Mag. (6) 11, 283.
RICH, G.R. (1951) Hydraulic Transients McGraw Hill.
RUSSELL, E.W. (1949) Unpublished ▓▓▓▓ Report.
SACK, R.A. (1946) Proc. Phys. Soc., 58, 729.
ST. VENANT (1867) J. Math. Pure & Appl. (2), 12, 237.
SCHMALTZ, G. (1936) Techn. Oberflachenkunde, Berlin.
STRAIN, R.N.C. (1955) Unpublished Work.
TABOR, D. (1957) Private Communication.
TAYLOR, G.I. (1946) J. Inst. Civil. Engrs. 26, 486.
TILLET, J.P.A. (1954) Proc. Phys. Soc., 67, 677.
TIMOSHENKO, S. (1951) Theory of Elasticity. McGraw Hill.
TOLANSKY, S. (1944) Phil. Mag., 35, 120.
             (1945) Proc. Roy. Soc. A., 184, 41.
             (1946) Ibid., 186, 261.
             (1948) Multiple Beam Interferometry. Oxford.

REFERENCES - continued

TOLANSKY, S. (1952) Zeits. f. Electrochemie 56, 263.
           (1955) An Introduction to Interferometry,
        Longmans.
TRESCA, H. (1864) C. R. Acad. Sci. Paris 59(2), 754.
VALKENBURG, M.E. VAN, CLAY, W.G. & HUTH, J.H. (1956) J. App.
        Phys. 27, 1123.
VINCENT, J.H. (1900) Proc. Camb. Phil. Soc., 10, 332.
WAGSTAFF, J.E.P. (1924) Proc. Roy. Soc. A. 105, 544.
WALTON, W.H. & PREWETT, W.C. (1949) Proc. Phys. Soc. B.,
        62, 341.
WHIFFEN, A.C. (1948) Proc. Roy. Soc. A. 194, 300.
WHITE, M.P. & GRIFFIS, Le Van. (1948) J. App. Mechs. 15, 256.
WILCOCK, W. (1951) Ph.D. Thesis. Manchester.
WORTHINGTON, A.M. (1877) Proc. Roy. Soc., 25, 260.
ZENER, C. (1941) Phys. Rev. 59, 669.

ACKNOWLEDGEMENTS